JOURNAL OF GEOPHYSICAL RESEARCH, VOL. 103, NO. B12, PAGES 30,287-30,309, DECEMBER 10, 1998

Magnetotelluric imaging of the Society Islands hotspot

Rita Nolasco and Pascal Tarits
Unité Mixte de Recherche, CNRS "Domaines Océaniques"
Institut Universitaire Européen de la Mer, Université de Bretagne Occidentale, Plouzané, France

Jean H. Filloux
Scripps Institution of Oceanography, La Jolla, California

Alan D. Chave
Department of Geology and Geophysics, Woods Hole Oceanographic Institution, Woods Hole, Massachusetts

Abstract. In April-June 1989, seafloor magnetotelluric data across and along the leading edge of the Tahiti hotspot were obtained. The magnetotelluric response functions were found to be strongly influenced by bathymetric and island effects, and a new procedure for modeling and removing this distortion using a thin sheet approach combined with the measured water depths is introduced. The corrected response functions are consistent with a two-dimensional structure. Inversion of the data shows a slightly higher conductivity (relative to a reference site located away from the hotspot) down to 130 km depth beneath the active area southeast of Tahiti underlain by a more resistive structure. There is a suggestion for a change in conductivity in the 400-450 km depth range, which is consistent with elevated temperatures. This result is consistent with a mantle plume of limited extent (less than 150 km radius) located near the leading edge of the Tahiti hotspot. The magnetotelluric data provide no evidence for lithospheric thinning or for a strong thermal influence over a large area, as would be required by a superswell model.

1. Introduction

Volcanoes are ubiquitous features of plate boundaries that are intimately linked to the processes of plate creation and consumption. However, there are about 50 other volcanic centers scattered about the globe which lack a clear association with plate boundaries. In ocean basins formed at slow spreading ridges such as the Atlantic, these volcanic islands tend to occur singly or in small groups associated with aseismic ridges, whereas in basins created at fast spreading ridges such as the Pacific, they commonly occur in linear chains [*Burke and Wilson*, 1976]. The Hawaiian and Society Islands chains are classic examples of the latter.

Wilson [1963] and *Morgan* [1971] proposed a model for the origin of such volcanic features which involves a fixed magma source or plume or hotspot in the mantle over which the oceanic plate moves. Intraplate volcanism results from the interaction of the plume with the overriding lithosphere. The resulting chain of volcanoes is oriented in the direction of true plate motion and has increasing age with distance from the spreading center. The numerous linear island chains in the central Pacific are perhaps the most prominent manifestation of long-lived hotspot activity.

Although the signatures of plume-lithosphere interaction are abundant on the Earth's surface, the dynamics of the associated mantle processes are poorly understood. Little direct information is available about the size and the shape of the plumes, their upwelling velocity, their source depth, or the initial depth of melting. For example, plumes have been hypothesized to originate at a thermal boundary layer in the transition zone [e.g., *Knittle et al.*, 1986] or at the core mantle boundary [e.g., *Moberly and Campbell*, 1984], but data to constrain these models are meager. In addition, numerous models of plume-lithosphere interaction have been proposed [e.g., *Sleep*, 1987; *Ribe and Christens*, 1994; *Phipps Morgan et al.*, 1995]. These models also depend strongly on poorly constrainted parameters such as the initial depth of melting or the size of the plume and its shape.

Plume-induced hotspot swells are well-defined bathymetric features associated with intraplate volcanic chains. Their origin is still controversial. Models for the origin of swells rely on combinations of three factors. First, some type of reheating mechanism resets the temperature in the lower part of the lithosphere to that of the asthenosphere. This in turn resets the effective thermal age of the oceanic lithosphere to a younger age (~ 25 Ma [*Crough*, 1978; *Detrick and Crough*, 1978]). Second, the

Paper number 98JB02129.
0148-0227/98/98JB-02129$09.00

lithosphere must be dynamically supported by mantle upwelling [*Parsons and Daly*, 1983; *Ribe and Chistens*, 1994]. Finally, the lithosphere must be underplated by a lighter mantle residue left after the extraction of melt from the uppermost oceanic mantle to maintain the anomalous elevation of the swell [*Robinson*, 1988]. The underplating may also originate from basaltic magma solidified within the lithosphere or deeper [*Phipps Morgan et al.*, 1995].

There is a definite need for more direct observations of mantle structure beneath active hotspots. However, most geophysical studies lack the necessary resolution to detect plume signatures. A mantle plume has been observed directly using seismic tomography only under the Iceland hotspot between 100 and 400 km depth [*Wolfe et al.*, 1997]. *Wolfe et al.* [1997] estimate that the plume could be of the order of 300 km in diameter with a temperature contrast between the plume and surrounding mantle of about 200-300°C. Comparable direct observations beneath a midplate hotspot are presently lacking.

In this paper, the results of a magnetotelluric mantle imaging experiment beneath an active hotspot in French Polynesia (Figure 1a) are reported. In section 2, the regional geologic setting and location of the seafloor electromagnetic data are outlined. In section 3, data processing and the procedure used to remove the strong distorting effects of seafloor bathymetry and islands are described in detail. Modeling and inversion results of the corrected data are given in section 4. Section 5 discusses the interpretation of the results in terms of mantle structure and the implications of this experiment for models of hotspots.

2. Geological Setting and Data

The islands of French Polynesia extend over approximately 5×10^6 km^2 in the South Pacific (Figure 1a). French Polynesia can be divided into five groups of islands (Marquesas, Tuamotu, Gambier, Society, Austral) which trend roughly subparallel and strike nearly perpendicular to the East Pacific Rise. These islands are generally interpreted to be the result of the interaction of the lithosphere with one or more hotspots [*Pautot*, 1975; *Duncan and McDougall*, 1976; *McDougall and Duncan*, 1980; *Duncan and Clague*, 1985]. The Society Islands alignment is N120°E, which is nearly the spreading direction (N115±5°E) of the Pacific plate in

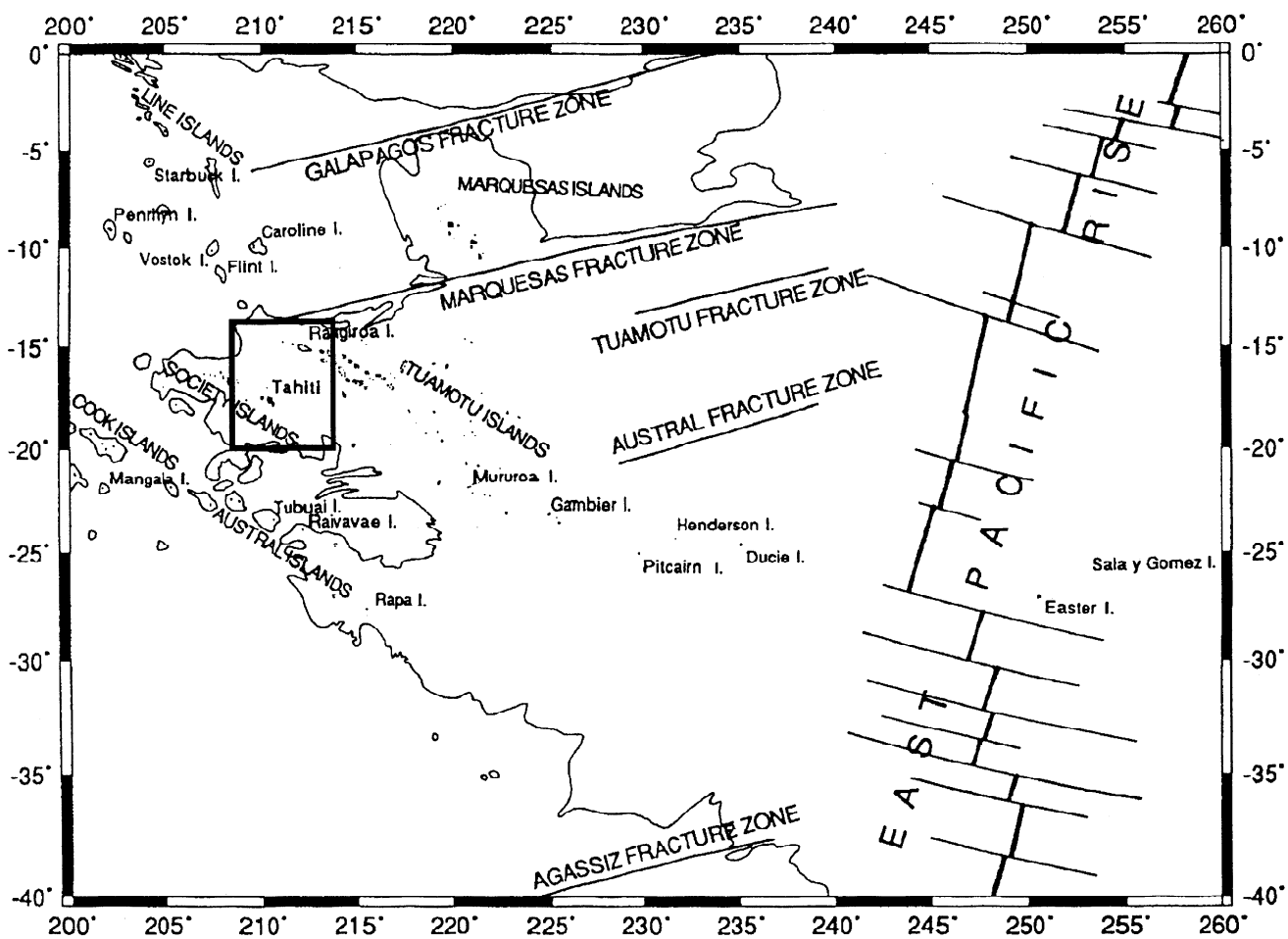

Figure 1a. Map of the South Pacific showing the location of the major tectonic features. The 4500m isobath is indicated, giving a rough idea of the extent of the postulated superswell [*Filmer et al.*, 1993].

a hotspot reference frame [e.g., *Diraison et al.*, 1991]. This is supported by the observed 11 cm/yr rate of along-chain migration of volcanic activity which is in good agreement with the absolute motion of the Pacific plate relative to a hotspot fixed to the mantle [*Duncan and McDougall*, 1976; *Jarrard and Clague*, 1977]. The age progression of the Society Islands volcanics in the strike direction ranges from 0 to 4.8 Ma, which have been emplaced on 70±5 Ma lithosphere [*Duncan and McDougall*, 1976].

The distribution of islands and seamounts is also controlled by old discontinuities in the oceanic lithosphere generated at the Farallon ridge [*Mammerickx et al.*, 1980], as indicated by the N160-170°E and the N70-80°E direction also observed in the geographical distribution of the islands (Figures 1a and 1b) in addition to the main N120°E strike. These directions correspond to the accretion of the Farallon ridge and to its associated transform faults, respectively [e.g., *Pautot*, 1975; *Diraison et al.*, 1991].

French Polynesia is set over an area termed the South Pacific superswell by *McNutt and Fisher* [1987] owing to the regional presence of shallower seafloor than would be expected based on lithospheric age (20-90 Ma), along with an unusually dense concentration of hotspots. This area is associated with low shear wave velocity [*Su*, 1992] extending through most of the upper mantle from the surface down to 450 km, a geoid low [*McNutt and Judge*, 1990], and possibly low elastic plate thickness [*McNutt and Menard*, 1978; *Calmant and Cazenave*, 1986; *Calmant*, 1987] with respect to the empirical elastic thickness versus age relationship [*Watts*, 1978; *Watts et al.*, 1980; *Calmant and Cazenave*, 1987]. These phenomena have been interpreted to reflect a combination

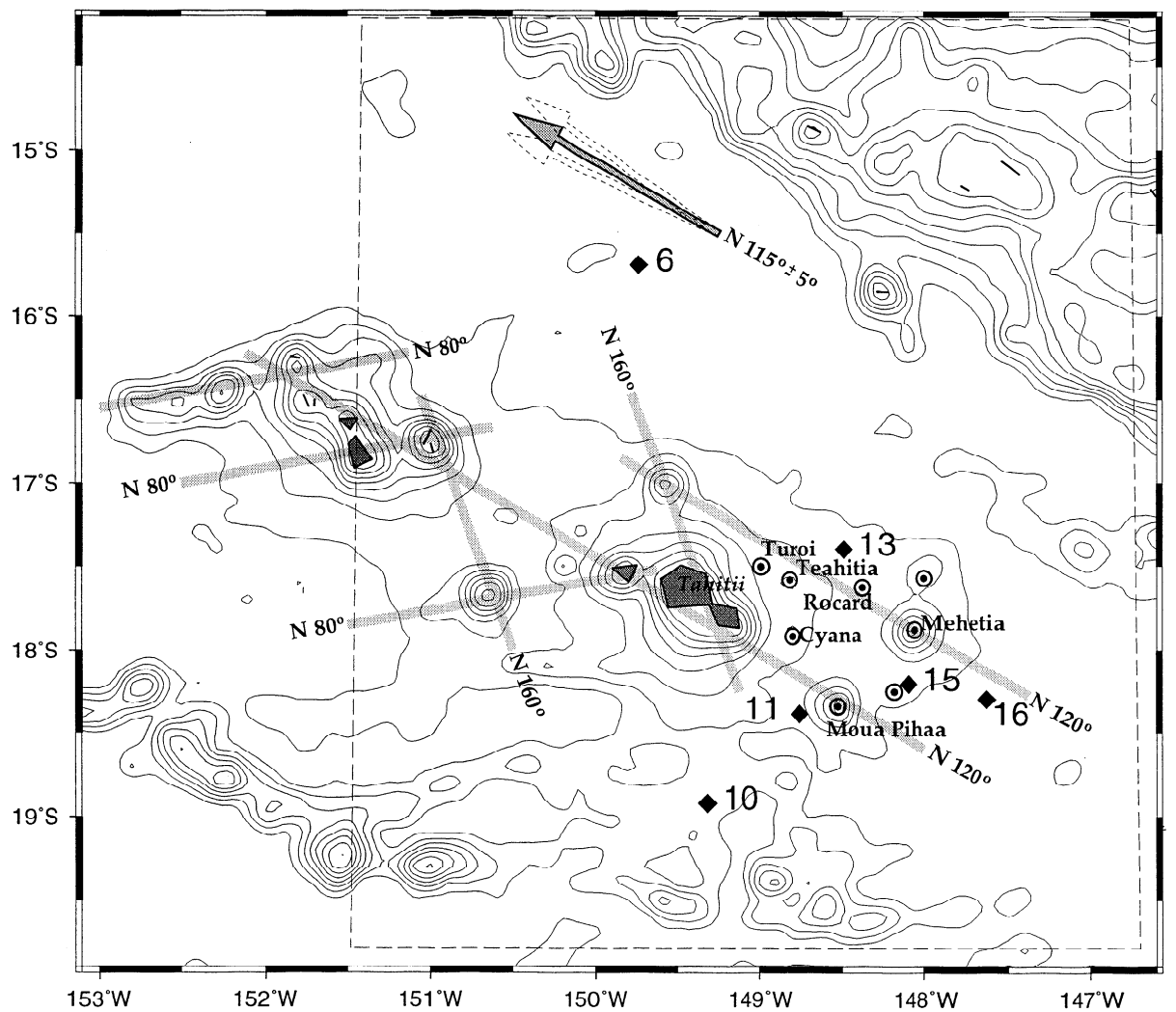

Figure 1b. The locations of the ocean bottom electromagnetic sites are superimposed on the bathymetry, with contours shown every 500 m. The circles are major volcanoes in the active Society hotspot region. The spreading direction is shown by the arrows. The surface expression of the hotspot activity is controlled by the N115±5°E drift direction of the Pacific plate and by the old structural discontinuities of the oceanic crust generated at the Pacific-Farallon ridge, i.e., the N160°-170°E direction parallel to the accretion axis and the N70°- 80°E direction of transform faults.

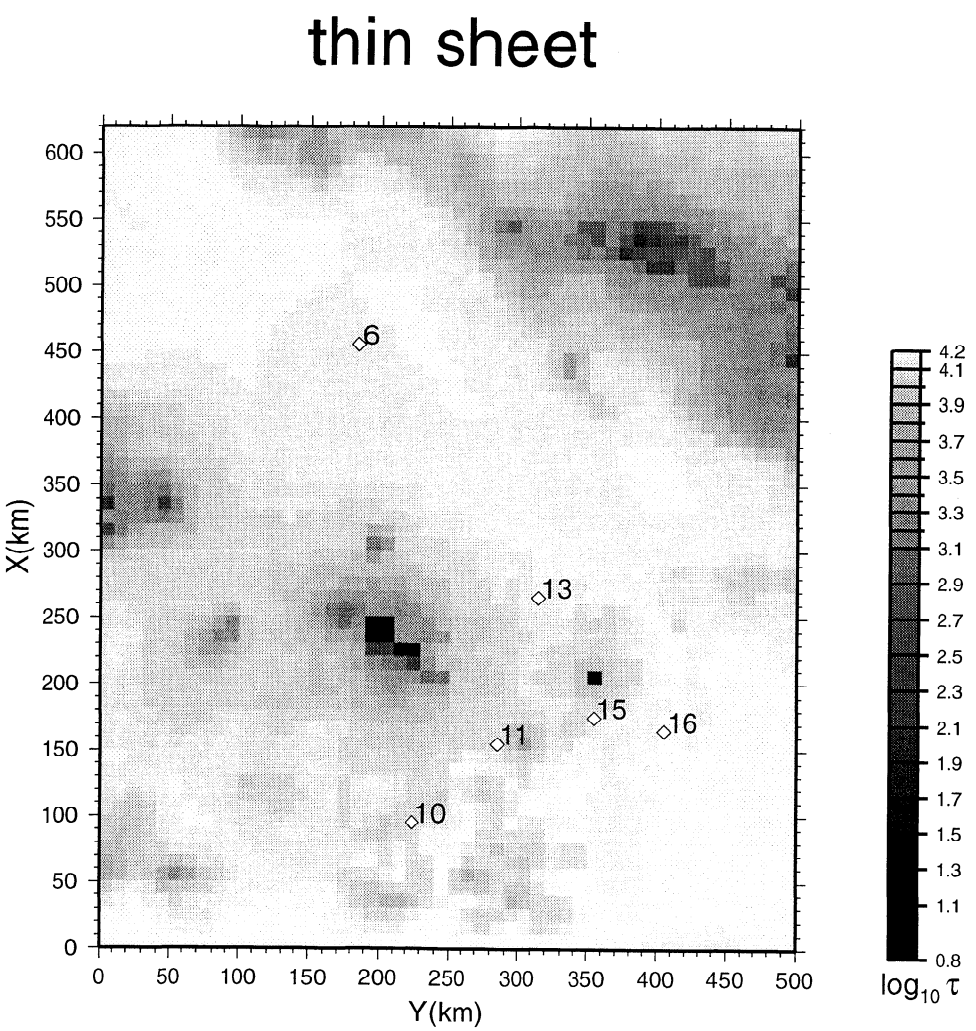

Figure 1c. A conductance model derived from the bathymetry shown in Figure 1b (dashed box). See text for details.

of lithospheric reheating, thinning and dynamic uplift due to ascending mantle flow [e.g., *McNutt and Fisher*, 1987; *McNutt and Judge*, 1990]. However, *Stein and Abbott* [1991] observe that the heat flow in this region, as a function of plate age, is not resolvably different from other Pacific values. In addition, *Filmer et al.* [1993] argue that the elastic strength of the superswell lithosphere is not everywhere anomalous. Other investigators [*Cazenave et al.*, 1980; *Filmer et al.*, 1993] have suggested that the Society Islands overlie a lithosphere of nearly normal elastic thickness even at the superswell maximum.

The current position of the active hotspot is located near the seismically active zone of Teahitia-Mehetia-Moua Pihaa at the southeastern end of the Tahiti lineation or about 60-130 km southeast of the island of Tahiti (Figure 1b) [*Okal et al.*, 1980; *Talandier and Okal*, 1984; *Cheminée et al.*, 1989; *Hékinian et al.*, 1991]. Mehetia is the easternmost island in the chain (Figure 1b). Teahitia, Moua-Pihaa, Rocard, and Cyana are active volcanoseismic seamounts. These seamounts have been identified by frequent seismic swarms and confirmed by bathymetric surveys [*Talandier and Kuster*, 1976; *Cheminée et al.*, 1989; *Hékinian et al.*, 1991].

While there is clearly surface evidence for active magmatic processes beneath the southeastern extreme of the swell, quantitative information on its depth of origin and the extent of melting is presently meager. In an attempt to address these issues, a set of seafloor magnetotelluric instruments were deployed over and around the active zone of the Society Islands swell from early April to mid-June 1989. In order to adequately describe the active area while also being able to characterize deep structure on a larger scale, the magnetotelluric instruments were placed in a tight cluster around the active area with an additional remote site placed to the northeast toward the Tuamotu chain (Figure 1b). Instruments were deployed for nine magnetotelluric soundings consisting of simultaneous measurements of the fluctuating horizontal electric and three component magnetic fields, as summarized in Table 1. Of these, complete magnetotelluric (MT) data were recovered from the six sites shown in Figure 1b, with only either electric or magnetic field data available from the remaining three

Table 1. Site Information

Station	Electric (E)/ Magnetic (M)	Duration, hours	Latitude, S	Longitude, W	Depth, m	Comment
S 6	E/M	1621/1620	15°41'	149°48'	4216	
S 10	E/M	1541/1540	19°01'	149°18'	3905	
S 11	E/M	1559/1560	18°18'	148°48'	2841	
S 12	E	1600/ - - -	17°48'	148°33'	3875	M lost
S 13	E/M	1600/1580	17°23'	148°24'	3910	
S 14	E	1560/ - - -	16°41'	147°56'	4230	M lost
S 15	E/M	1600/1580	18°06'	148°12'	3875	
S 16	E/M	1561/1560	18°18'	147°41'	4203	
S 17	M	- - - /1560	17°30'	148°52'	3334	E lost

Resolution of the electric is 3 nV/m and magnetic is 0.1 nT. Sampling rate in 64 per hour.

sites. In addition, measurements of the bottom pressure fluctuations at eleven sites were obtained and will be reported elsewhere.

The instrumentation used is described by *Filloux* [1987]. Magnetic field variations were measured by optical detection of the zero point of a magnet suspended on a taut tungsten fiber and enclosed in a nulling coil. The electric field is determined from continuous recording of the electric potential between a pair of silver-silver chloride electrodes connected to seawater through a 6 m-long salt bridge. Electrode drift is rejected by reversing their connections to a salt bridge with a electromechanical chopper. Both the electric and magnetic fields were sampled at a rate of 64 per hour.

3. Data Processing and Island/Bathymetry Distortion

3.1. Data Processing

The electric and magnetic field time series were transformed into the frequency domain 2x2 magnetotelluric response tensor relating the horizontal electric and magnetic fields using an extension of the robust remote reference method of *Chave and Thomson* [1989]. This approach is based on the division of a long time series into shorter sections prior to Fourier transformation, followed by estimation of the responses with a robust least squares method to eliminate the influence of outliers in the electric and leverage points in the magnetic field. A nearby seafloor magnetic site was used as a remote reference to eliminate bias due to uncorrelated noise in the local magnetic field. The principal extensions to the method of *Chave and Thomson* [1989] include (1) the use of variable section lengths such that the frequency of interest is always of order the inverse section length, (2) implementation of leverage control to eliminate anomalous magnetic field data based on the size of the hat matrix diagonal as described by A. D. Chave and D. J. Thomson (On the robust estimation of magnetotelluric response functions, manuscript in preparation, 1998), and (3) use of the nonparametric jackknife to estimate confidence intervals on the responses. *Thomson and Chave* [1991] give the complete theory for the jackknife in a spectral analysis context, and demonstrate its greater accuracy as compared to parametric approaches in the presence of outliers or mixtures of distributions, as frequently occurs in electromagnetic induction.

At each of the six sites shown in Figure 1b, the four complex elements of the magnetotelluric response tensor were computed as a function of frequency using this approach. These quantities will henceforth be regarded as the data.

The transfer functions between the vertical and horizontal magnetic components (Z/B) were also computed, but there is a substantial difference between the results obtained with daytime and nighttime data. Furthermore, the Z/B response is sensitive to the choice of a remote reference site. This suggests significant source field effects on the Z/B response, probably due to proximity to the equatorial electrojet. For these reasons, the Z/B responses will not be further considered in this paper.

3.2. Removal of Island and Bathymetry Distortion

The seafloor electromagnetic field was expected to be strongly distorted by the presence of many islands and the rugged bathymetry in the Tahiti region (Figure 1b). This presents significant modeling difficulties, as it is numerically difficult to simultaneously resolve the small-scale (relative to the induction scale) bathymetry that produces distortion and yet include the much larger scale and presumably heterogeneous structures of the underlying mantle. The now standard approach to this problem is the application of a tensor decomposition model to the observed magnetotelluric response to remove galvanic distortion due to small scale structure and recover the regional response [e.g., *Groom and Bailey*, 1989; *Chave and Smith*, 1994]. However, these methods consistently fail to yield a statistically acceptable fit to the Tahiti data at all periods even when magnetic field galvanic distortion, which is typically large for seafloor data [*White et al.*, 1997], is included, suggesting a breakdown of the tensor decomposition model assumptions. In particular, it is unlikely that the re-

gional electric field remains uniform across the large heterogeneities observed in the Tahiti area or that the electric field at the inhomogeneity can be approximated by its value at the observation point. As shown by *Chave and Smith* [1994], these assumptions are implicit in the use of a tensor decomposition, and their violation will lead to poor tensor decomposition fits. In addition, tensor decomposition methods implicitly assume that self-induction is negligible, and that condition is not appropriate for much of the Tahiti data.

Accordingly, a hybrid approach has been applied to distortion removal in which the bathymetric influence is first modeled as accurately as possible and removed from the data, and the ensuing corrected responses which reflect mantle structure are then available for interpretation. Assuming time dependence, the integral equation governing scattering of the electric field by a conductive heterogeneity is [*Weidelt*, 1975]

$$\mathbf{E}(\mathbf{r}) = \mathbf{E}_m(\mathbf{r}) - i\omega\mu \int_V \delta\sigma(\mathbf{r}')\mathbf{G}(\mathbf{r},\mathbf{r}')\mathbf{E}(\mathbf{r}')d\mathbf{r}' \quad (1)$$

where V refers to the volume of the distorting body, $\mathbf{G}(\mathbf{r},\mathbf{r}')$ is the whole space Green dyadic, $\delta\sigma$ is the conductivity anomaly relative to the background value σ_o, and $\mathbf{E}$ is the observed electric field. The two terms on the right-hand side of (1) are the background electric field in the absence of the heterogeneity and the scattered electric field, respectively, which includes both the inductive and the galvanic parts. Applying Ampere's law to (1) gives an analogous integral equation for the magnetic field

$$\mathbf{B}(\mathbf{r}) = \mathbf{B}_m(\mathbf{r}) + \mu \bigtriangledown \times \int_V \delta\sigma(\mathbf{r}')\mathbf{G}(\mathbf{r},\mathbf{r}')\mathbf{E}(\mathbf{r}')d\mathbf{r}' \quad (2)$$

Equations (1)-(2) may be written in tensor form by approximating the integrals by sums to give

$$\mathbf{E} = \mathbf{E}_m + \mathbf{M}\mathbf{E} \quad (3)$$

$$\mathbf{B} = \mathbf{B}_m + \mathbf{K}\mathbf{E} \quad (4)$$

where position dependence of the variables has been dropped. For galvanic distortion of the electromagnetic fields, the elements of $\mathbf{M}$ and $\mathbf{K}$ are real and frequency independent, but these conditions do not hold in general. The desired mantle response $\mathbf{Z}_m$ is the solution of

$$\mathbf{E}_m = \mathbf{Z}_m\mathbf{B}_m \quad (5)$$

while the observed magnetotelluric response satisfies

$$\mathbf{E} = \mathbf{Z}_o\mathbf{B} \quad (6)$$

Combining (5)-(6) with (3)-(4) and rearranging the terms yields

$$\mathbf{Z}_m = (\mathbf{I} - \mathbf{M})(\mathbf{I} - \mathbf{Z}_o\mathbf{K})^{-1}\mathbf{Z}_o \quad (7)$$

where $\mathbf{I}$ is the identity tensor. Equation (7) gives the mantle response in terms of the observations once the elements of $\mathbf{M}$ and $\mathbf{K}$ are known.

In the ocean at long periods where the skin depth is large compared with the water depth, the thin sheet approximation given by *Vasseur and Weidelt* [1977] may be applied. While $\mathbf{E}$ and $\mathbf{M}$ are essentially the same at the sea surface and seafloor, $\mathbf{B}$, $\mathbf{B}_m$, and $\mathbf{K}$ are decidedly different. The elements in $\mathbf{M}$ and $\mathbf{K}$ may be computed numerically from the measured bathymetry around Tahiti using a thin sheet of spatially variable conductance to simulate the ocean. The relevant equations may be derived directly from (1)-(2). Under the approximation, integrating (1) through the ocean gives

$$\mathbf{E}_s(\mathbf{r}_s) = \mathbf{E}_{sm}(\mathbf{r}_s) - i\omega\mu \int_S \delta\tau(\mathbf{r}_s')\mathbf{G}_s(\mathbf{r}_s,\mathbf{r}_s')\mathbf{E}_\mathbf{S}(\mathbf{r}_s')d\mathbf{r}_s' \quad (8)$$

where S refers to the area of the thin sheet, $\mathbf{G}_s$ is the surface dyadic Green function which incorporates the relevant seafloor boundary conditons, $\mathbf{E}_s$ has only horizontal components, $\delta\tau$ is the anomalous conductance of the thin sheet which reflects horizontal variations in water depth, and $\mathbf{r}_s$ is a horizontal direction vector. A comparable expression for the magnetic field follows directly

$$\mathbf{B}(\mathbf{r}) = \mathbf{B}_m(\mathbf{r}) + \mu \int_S \delta\tau(\mathbf{r}_s')\mathbf{R}(\mathbf{r},\mathbf{r}_s')\mathbf{E}_\mathbf{S}(\mathbf{r}_s')d\mathbf{r}_s' \quad (9)$$

where $\mathbf{B}$ is the seafloor magnetic field and $\mathbf{R}$ is the curl of $\mathbf{G}_s$.

The large-scale bathymetry, including the outlines of the major islands, was taken from the digital ETOP05 database which has a resolution of about 9 km. The map was then locally corrected as needed with more detailed bathymetric data taken from *Cornaglia* [1995]. The result is shown in Figure 1b. The area between 151.5°W and 146.7°W and between 14.2°S and 19.8°S was discretized into square 10 by 10 km cells and converted into a conductance map. The conductance in a given cell is simply the water depth times an average seawater conductivity of 3.3 S/m. When a cell is dominated by land, a lower conductance bound of 7 S was used. The surface conductance map is shown in Figure 1c. The anomalous conductance which appears in (8)-(9) is the difference between the surface conductance and that for a uniform ocean of 4.5 km depth. The electric field is assumed constant within each conductance cell to yield the thin sheet form of (3)-(4). This in turn gives the elements of $\mathbf{M}$ and $\mathbf{K}$ from which the mantle magnetotelluric response may be obtained from (7).

The island and bathymetry (I/B) distortion model also depends on the conductivity structure of the mantle, as reflected in the boundary conditions incorporated in $\mathbf{G}_s$ and $\mathbf{R}$, but previous work has shown that mutual coupling between surficial inhomogeneities and deep mantle lateral heterogeneities is weak [e.g., *Menvielle et al.*, 1982; *Tarits and Menvielle*, 1983; *Terra*, 1993]. Hence the $\mathbf{M}$ and $\mathbf{K}$ tensors in (7) depend only weakly on details of the mantle structure and are mainly functions of the surface distorting features. This makes it feasible to compute them by assuming a one-dimensional (1-D) mantle taken from seafloor studies over lithosphere of similar age [*Filloux*, 1977, 1980; *Tar-*

its and Jouanne, 1990] underlying a nonuniform thin sheet simulating the surface features. We use a model with two layers over a half-space. The first layer is 100 km thick and its resistivity is 10^3 Ω m. The second layer is 300 km thick and its resistivity is 40 Ω m. The half-space resistivity is 2 Ω m. This yields $\mathbf{Z}_m$ provided that the real mantle is not too different from the 1-D model used to compute **M** and **K**. The validity of these assumptions were verified by reestimating the elements of **M** and **K** using the derived mantle models (see section 4), hence making the model process iterative. The difference between the **M** and **K** tensor estimated with the initial and final models is very small (<0.5% and <2% for **M** and **K**, respectively)

The confidence intervals on $\mathbf{Z}_m$ were calculated using the nonparametric jackknife [*Thomson and Chave*, 1991]. This is implemented by first computing the N delete one estimates of $\mathbf{Z}_o$ based on all N data segments except for the ith one. The delete one estimates of $\mathbf{Z}_o$ are then used with (7) to get N delete one estimates of $\mathbf{Z}_m$, which are in turn combined as described by *Thomson and Chave* [1991] to get its standard error. The confidence intervals follow by assuming Gaussian statistics, which is a reasonable model when the data are processed robustly.

4. Results

4.1. Reference Site 6

The magnetotelluric response at station S6, located about 350 km northwest of the leading edge of the swell (Figure 1b), was corrected for distortion due to bathymetery using the method described in section 3. Figure 2a compares the corrected (solid symbols) with the observed (open symbols) response tensor. After correction, the diagonal terms vanish within the statistical uncertainty at all 11 periods, while the antidiagonal coefficient are similar except for a change in sign. This is suggestive of but does not require a 1-D interpretation.

In accordance with the suggestion of *Berdichevsky and Dmitriev* [1976], the geometric mean of the antidiagonal terms of the corrected tensor was utilized to minimize the effects of any residual anisotropy. A necessary and sufficient condition for 1-D behavior of the response is the statistically adequate fit of a D^+ model [*Parker and Whaler*, 1981] to the data. With 11 frequencies, the expected value of the standardized χ^2 misfit is 22, while the D^+ misfit is 20, and hence a 1-D interpretation of the S6 data is justified. Using the criterion of *Parker* [1980], the maximum resolution depth is about 650 km (Table 2).

Of all possible models which fit a set of magnetotelluric data, the D^+ model is the best fitting but roughest one, and hence it is necessary to seek a model with a suboptimal fit which is more physically appealing. This requires the imposition of smoothness constraints, either explicitly for a nearly continuous model or by pursuing a model with a limited number of layers. A multilayer inversion based on the Bayesian method of *Tarits et al.* [1994] was employed with the algorithm left free to minimize the number of layers for a given misfit. The a posteriori probability density function (pdf) of the resulting model is obtained from the data pdf, taken to be Gaussian, times the a priori pdf imposed on the model parameters. The a priori pdf chosen is uniform so that a given parameter of the model (resistivity or layer depth) is selected with equal probability over a given interval. Table 3 summarizes the a priori pdf's. The resolution of the model parameters was determined using Bayesian

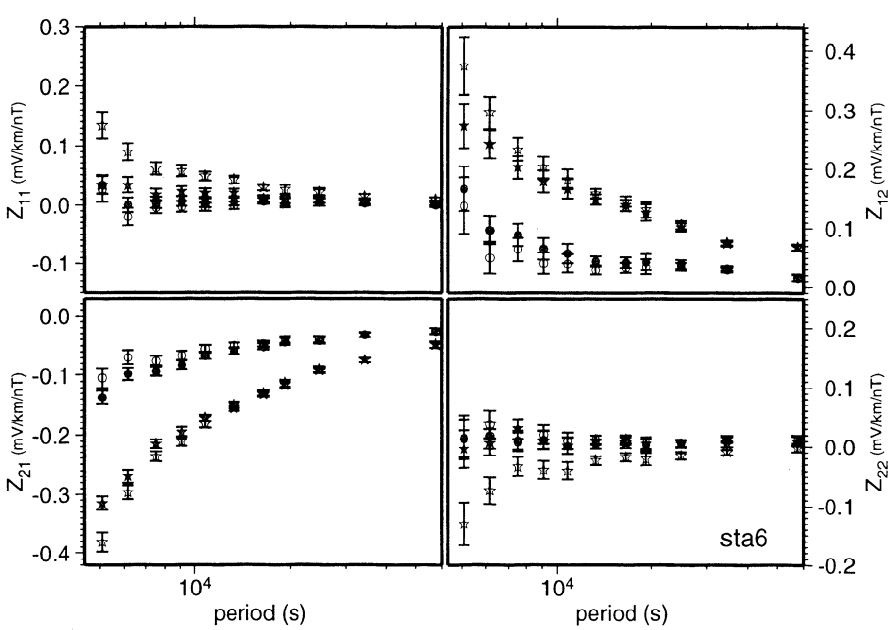

Figure 2a. The MT tensor at site S6, with the original values given by open and the derived mantle values given by solid symbols, respectively. The real and imaginary parts are denoted by circles and stars. The error bars are the double-sided 95% values.

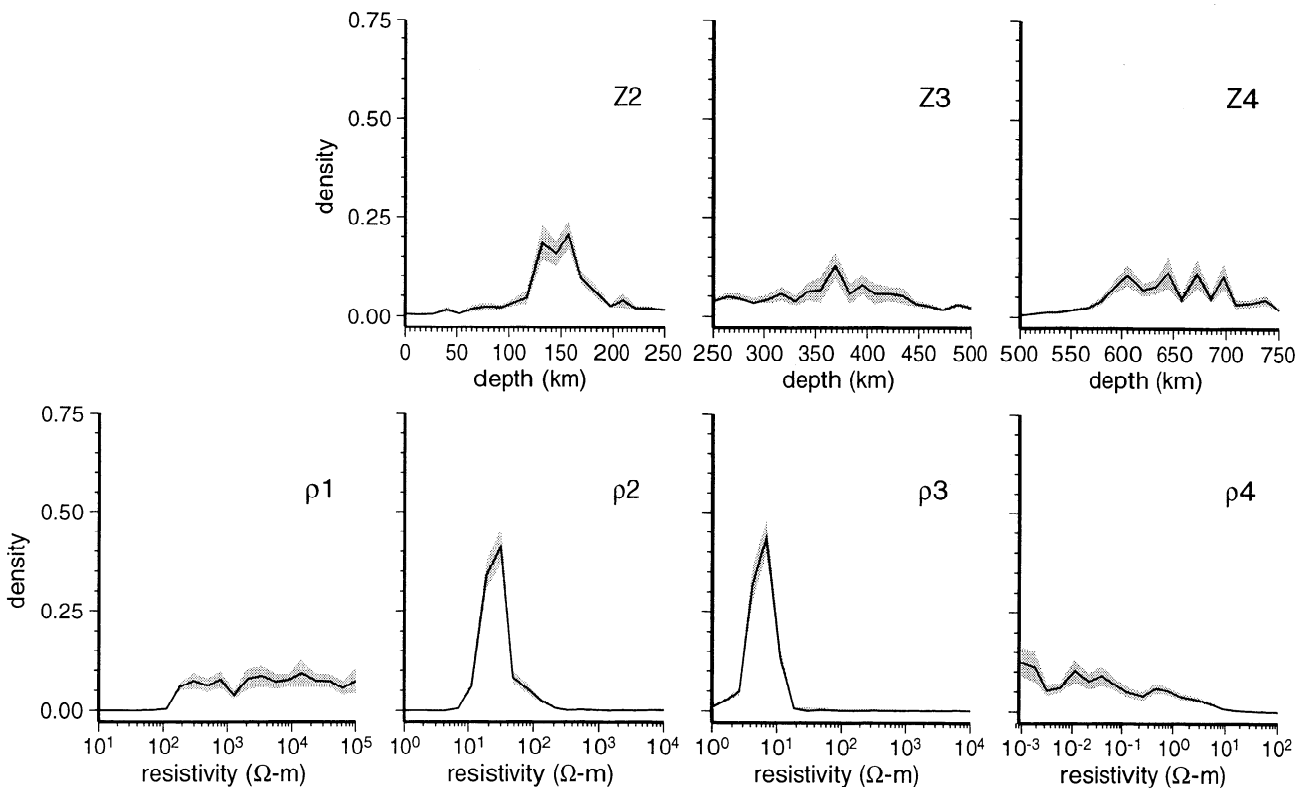

Figure 2b. Bayesian statistics inverson [*Tarits et al.*, 1994] of the mantle tensor at S6: marginal pdf's of the a posteriori law of the four-layer 1-D model parameters. The a priori intervals for each parameter are along the horizontal axes. The vertical axes represent the density of the marginal pdf normalized so the surface is one. The solid line joints the marginal pdf mean values and the dark area represent the standard deviation.

principles by means of the a posteriori marginal pdf's. The marginal pdf for each parameter of the model is calculated from the a posteriori pdf of the model and may be interpreted as the parameter pdf [*Tarits et al.*, 1994].

A model consisting of three layers above a homogeneous half-space resulted from this analysis (Figure 2b), with a standardized misfit of 22.5. The a posteriori expected values for the parameters are given in Table 3. The pdf for each resistivity and the depth of the base of each layer are depicted in Figure 2b. The first layer is 110-160 km thick with the next interface located between 360 and 410 km. Layer 3 extends down to 600-700 km. The resistivity of layer 1 has a lower bound of about 200 Ω m. Layer 2 has a resistivity centered at 18-30 Ω m, while layer 3 has a value of 6 Ω m. The resistivity of the half-space has an upper bound of 0.1-1 Ω m. This preliminary model will be refined in the process of the joint modeling of all of data.

Table 2. D^+ Inversion Model at Site 6

Depth, km	Conductance, S
189.	4,886.
405.	23,714.
653.*	- - -

*Depth below which a perfectly conductor half-space does not affect the model.

4.2. Distortion Correction at Remaining Sites

Using the reference model for site 6, revised **M** and **K** tensors at the remaining sites were computed as described earlier. Figure 3 shows both the observed MT tensors $\mathbf{Z}_o$ (open symbols) and the corrected (or mantle) response tensors $\mathbf{Z}_m$ (solid symbols). The jackknifed double-sided 95% confidence limits are also depicted. Some sites such as 11 and 13 display substantial changes, while at sites 10 and 16, the MT tensor is only altered slightly for some of the coefficients. Note that sites 11 and 13 are the closest sites to the island of Tahiti (see Figure 1b) and hence would be expected to experience the strongest distortion due to topography. In contrast, except for reference site 6, sites 10 and 16 are farthest from extreme large-scale topography, and hence its influence might be expected to be weak.

The directions for which the corrected MT tensor is antidiagonal at each site and the two antidiagonal terms which are the maximum and the minimum values, respectively, of the impedance for that direction, were calculated using the tensor decomposition proposed by *Counil et al.* [1986]. An alternate technique such as

Table 3. A Priori and a Posteriori Probabilities for Station 6

A Priori pdf		Expected Values	
Resistivity, Ω m	Depth, km	Resistivity, Ω m	Depth, km
10^{1}-10^{5}	0-250	4555.	150.
10^{0}-10^{4}	250-500	27.	369.
10^{0}-10^{4}	500-750	6.59	638.
10^{-3}-10^{2}		0.12 7	

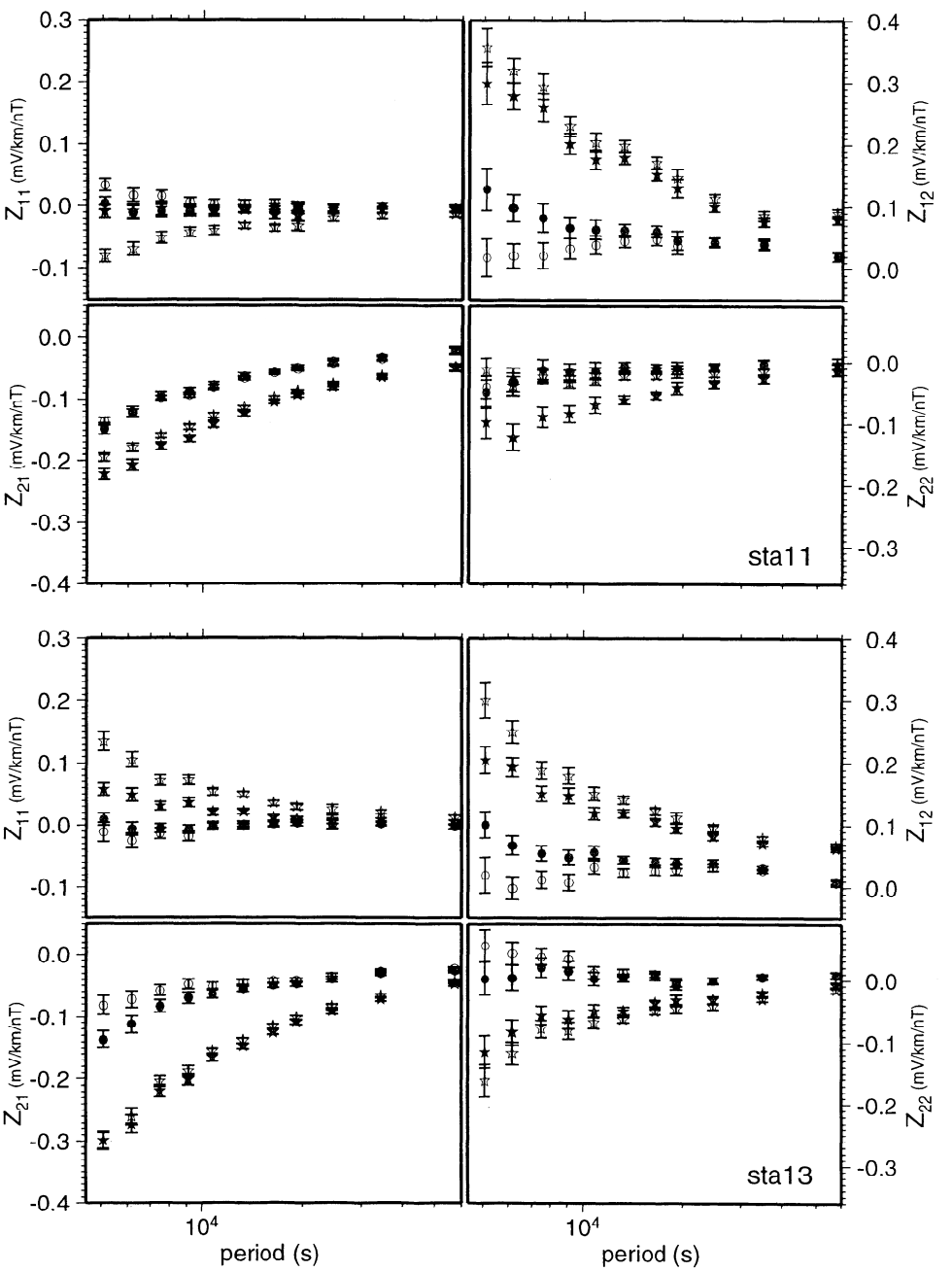

Figure 3. The original ($\mathbf{Z}_o$) and corrected or mantle responses ($\mathbf{Z}_m$) are shown for stations 15, 16, 13, 11, and 10. The symbols are defined in the Figure 2a caption. See text for details.

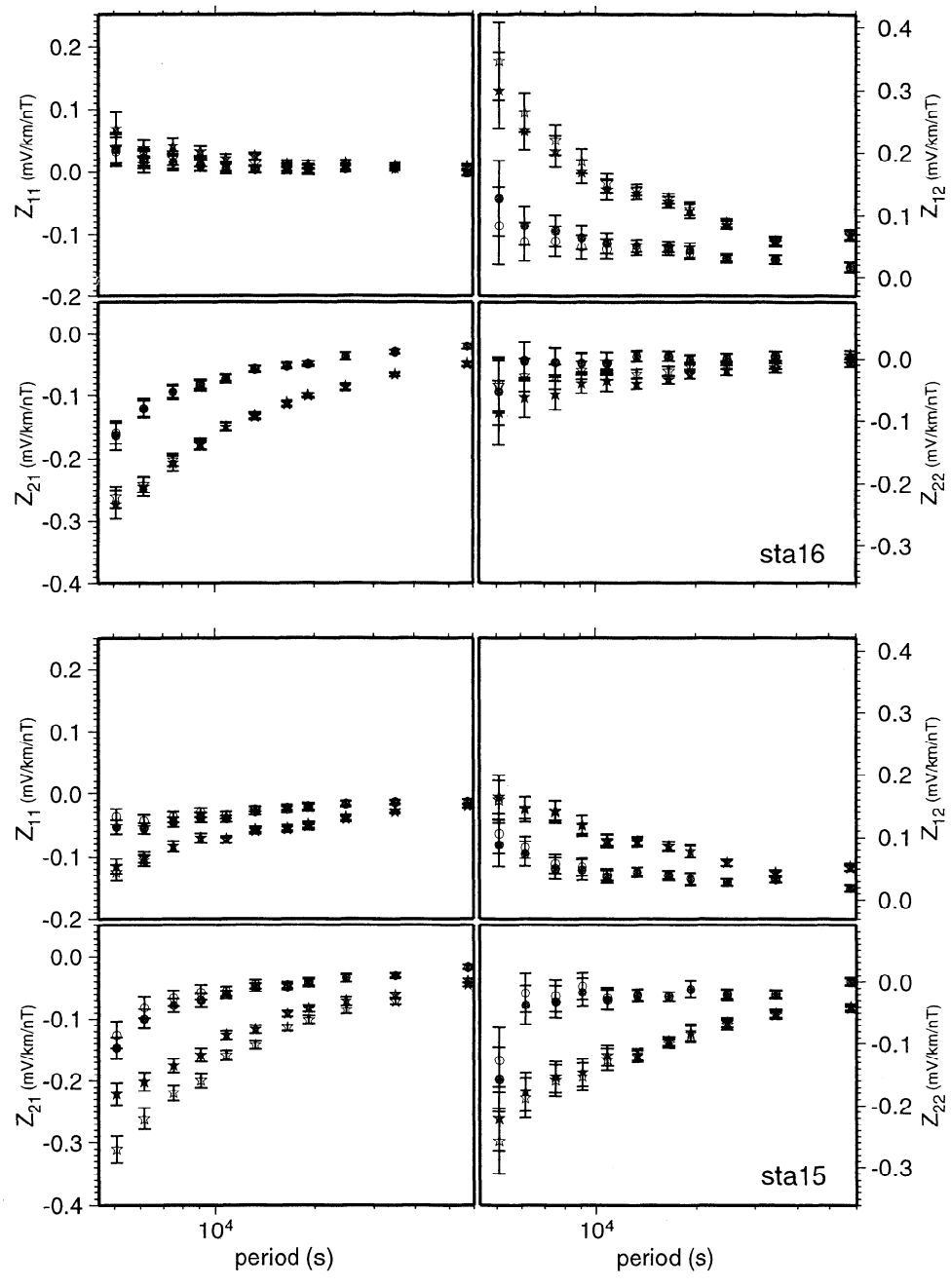

Figure 3. (continued)

that of *Vozoff* [1972] gives similar results. In Figure 4, we present the antidiagonal direction of the tensor. At all sites but S6, the direction is very stable with period except at the longest one. Site 6 does not show any preferential direction, which is consistent with the 1-D interpretation shown in the last section. The average direction for stations 16, 10, 11, and 13 is N130°E, in agreement with the general strike of the Society Chain (Figure 1b). There is some scatter left because the bathymetry is only modeled on a 10 by 10 km mesh. This can lead to substantial errors at some sites; see station 15, for instance, which is close to some very large seamounts. The skew at all sites is vanishingly small. Hence the corrected tensor behaves in a 2-D manner, with the transverse electric (TE) mode in the N130°E direction and the transverse magnetic (TM) mode in an orthogonal direction. When the stations (except for station 15) are projected onto a direction perpendicular to the strike of the island chain and the antidiagonal components of $\mathbf{Z}_m$ are examined, a reasonable 2-D profile is obtained Figure 5. The data at station 15 were left out because the directions of the tensor were significantly different from the mean N130°E strike chosen for the 2-D analysis. They will nevertheless be compared to the response of the final model to verify that the underlying hypotheses used to account for and get rid of

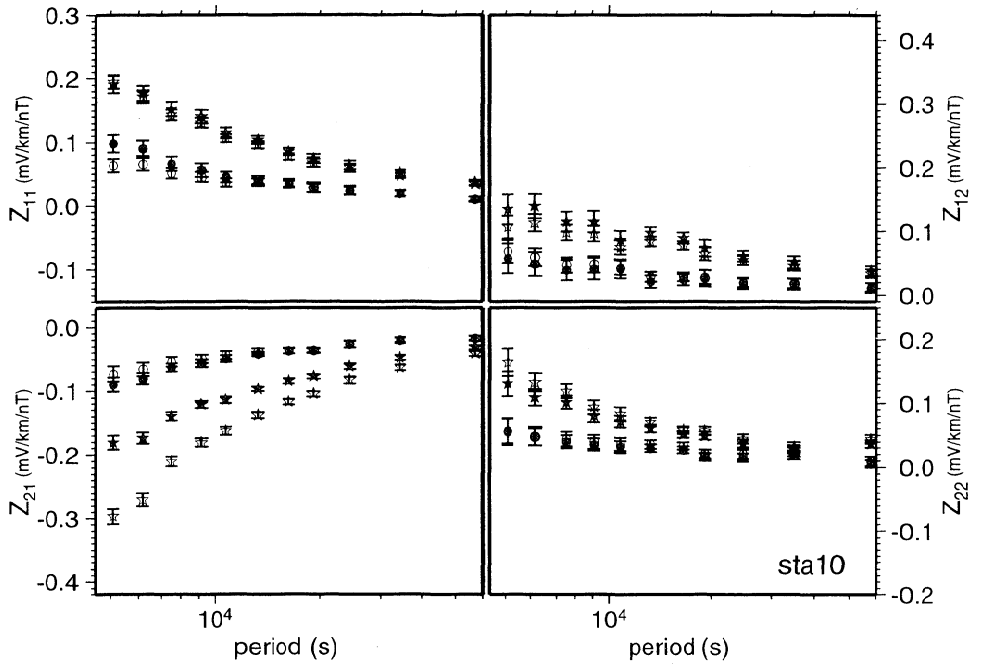

Figure 3. (continued)

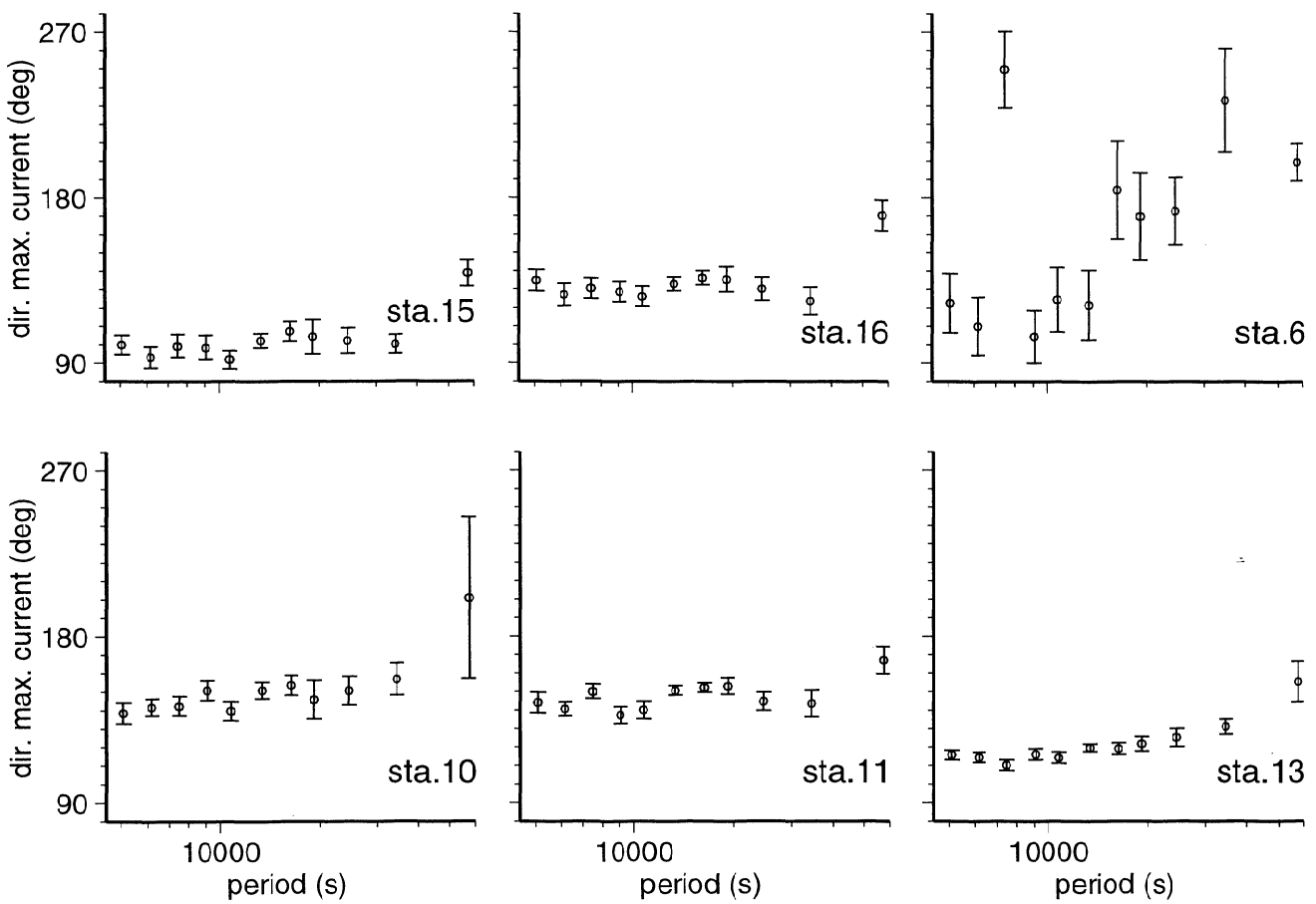

Figure 4. The direction of the maximum of $\mathbf{Z}_m$ as a function of period.

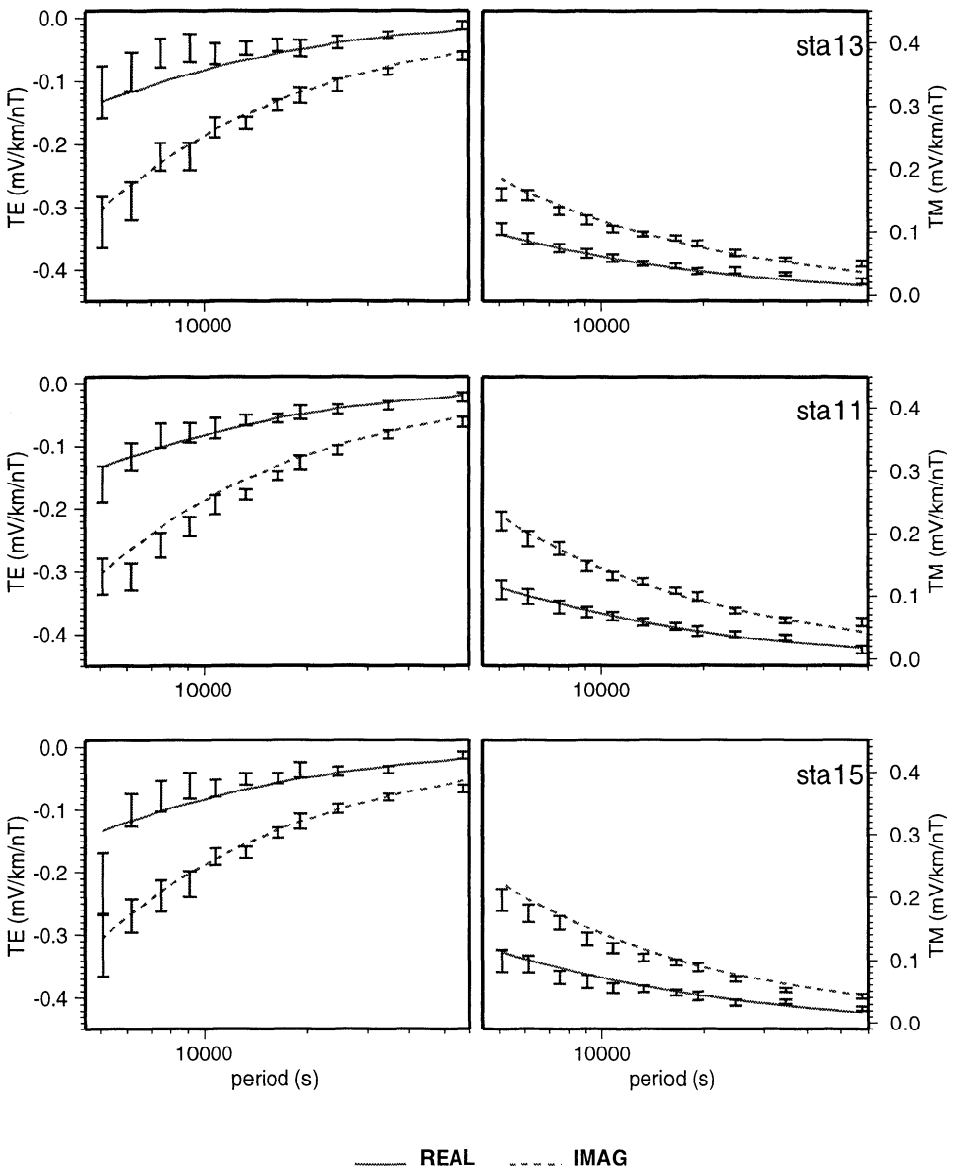

Figure 5. Fit for the results of two-dimensional model shown in Plate 1 and the corrected data tensor, for the TE mode (in N130°E direction) and the TM mode (in an orthogonal direction) for all sites.

the topographic effect are valid. In other words, it will be verified that the distortion is largely geometrical and weakly coupled to the mantle.

4.3. Modeling of the Corrected MT Tensor

4.3.1. Two-dimensional modeling. Modeling of the data was carried out by means of a finite difference 2-D code (P. Tarits, internal report, 1984) utilizing a χ^2 minimization algorithm based on a steepest gradient method [e.g., *Filloux*, 1979; *Fischer and LeQuang*, 1981]. The latter was selected on the basis of simplicity and robustness. The χ^2 misfit measures the difference between the observed and calculated real and imaginary parts of the TE and TM impedances. The penalty function actually minimized was the sum of the χ^2 misfit plus the squared norm of the log conductivity gradient times a damping parameter adjusted so that the regularizing term is smaller than the expected value of χ^2 (here 220) in order not to overemphasize the regularization.

As previously mentioned, only the S6, S10, S11, S13, and S16 data were used in the modeling procedure. The starting model was the 1-D model obtained at S6 described in section 4.2. The gridding for the modeling procedure is shown in Plate 1 (top). The finite difference gridding for each forward calculation was much finer in order to get an accurate response. It was based on classical rules of thumb in finite difference calculations [e.g., *Doucet and Pham Van Ngoc*, 1984], taking into account the frequency and the conductivity in all layers and prisms.

The best fit was obtained with the model shown in Plate 1 (bottom). The χ^2 misfit is 217. The station-by-station comparison between the model and the data is

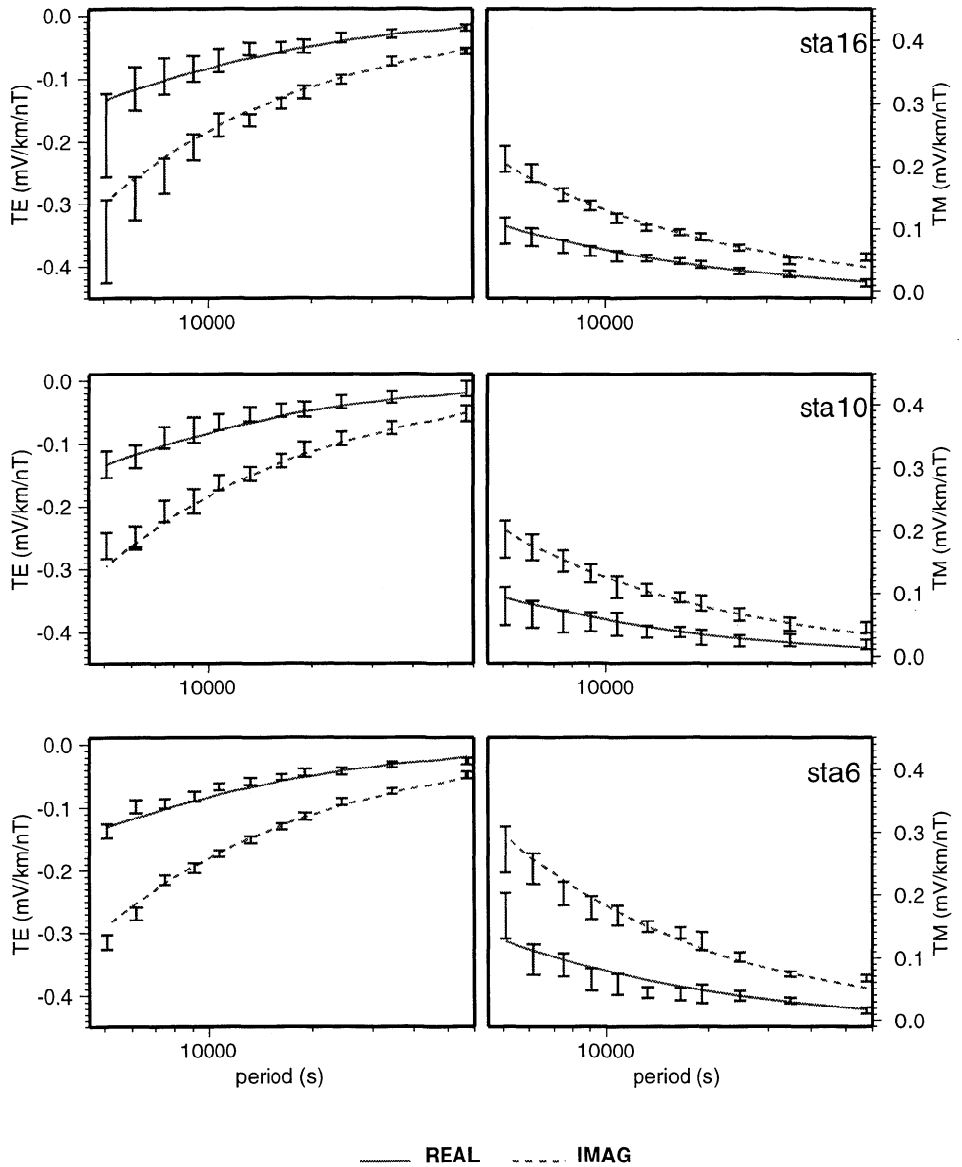

Figure 5. (continued)

presented in Figure 5. The fit is good everywhere except for the real part of the TE impedance at site S13 toward the short periods. There is no obvious explanation for the misfit at site S13. Nevertheless, one may suppose that the mesh used to describe the topography (10 by 10 km) was not fine enough to account for very local features. Figure 5 also shows a comparison between the S15 mantle tensor and the model calculated at the position corresponding to the projection of station S15 onto the profile. The fit here is also adequate.

The resolution of the model parameters (including the 1-D structure under site S6, which was refined in the 2-D minimization procedure) was tested by first fixing the size (width and thickness) of the blocks in the heterogeneous part of the model (Plate 1, bottom) and the thickness of the layers in the 1-D model on the sides and then computing the change in the fit as each resistivity value was changed with all of the others being held constant. The procedure was then repeated by fixing the resistivities and the widths of the blocks and changing the block thicknesses. The results are depicted in Figure 6. Figure 6a shows the variation of the rms misfit with respect to changes in the resistivity of each block in the central part of the model where the structure is quite heterogeneous (see Plate 1). The resistivity used in the model, presented in Plate 1 (bottom), is depicted with a star in Figure 6. Most of the resistivity values are fairly well constrained. In the worst case, the range is within an order of magnitude at the 95% confidence level. Only the resistivity in block 15 is poorly resolved. The misfit for the 1-D structure at site S6 is presented in Figure 6b. Except for the underlying halfspace (extreme right), the resistivities are again fairly well resolved.

There is usually a trade-off between the determination of the resistivity and the thickness of a given block.

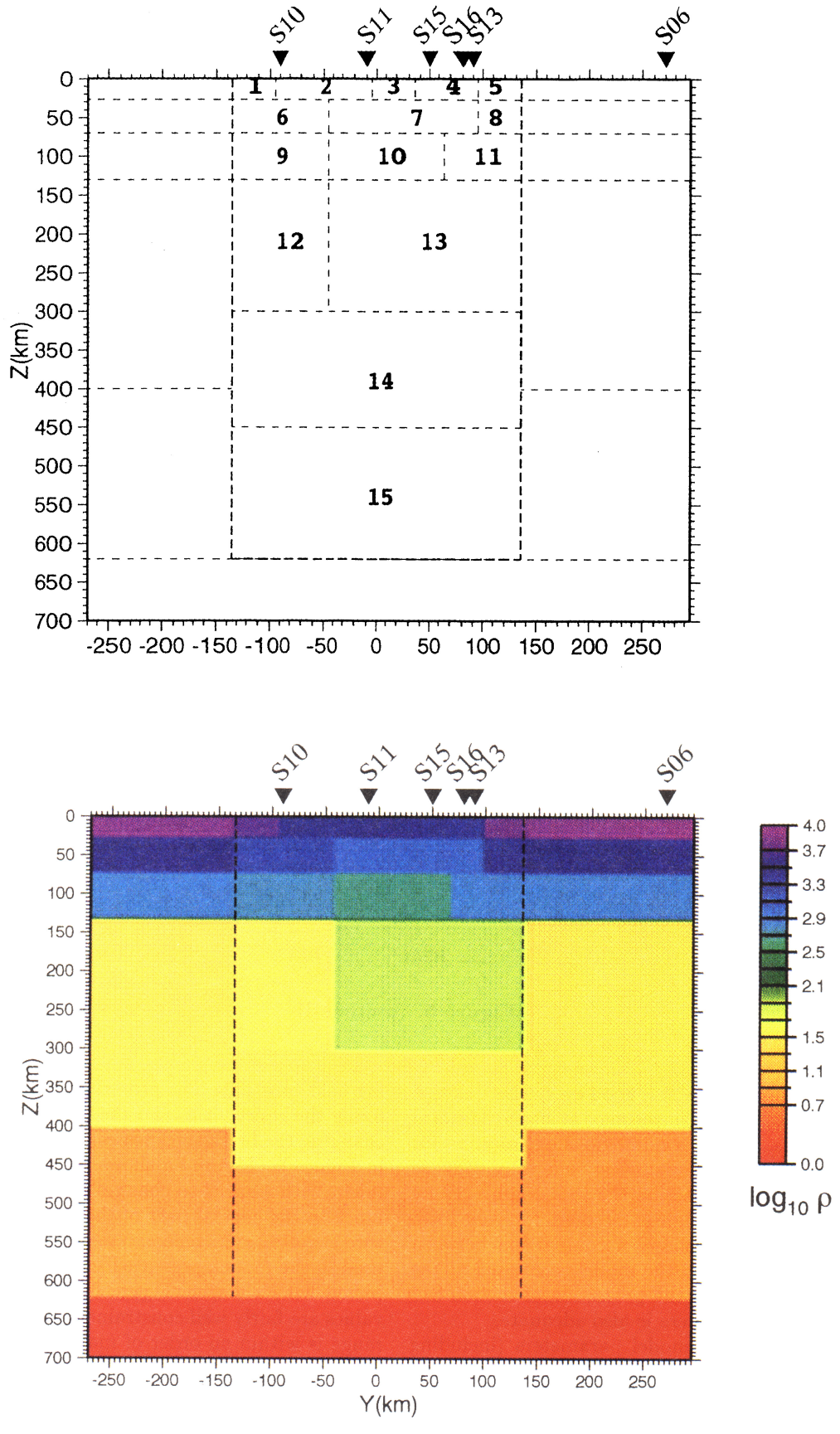

Plate 1. Two-dimensional southwest-to-northeast electrical model (strike in N130°E direction), which best fits the data. A 1-D layered medium symetrical with respect to the central heterogeneous area was assumed The localization of the station over this heterogeneous area is noted. (top) The gridding of the model. (bottom) The model with a color scale in log of resistivity (Ω m).

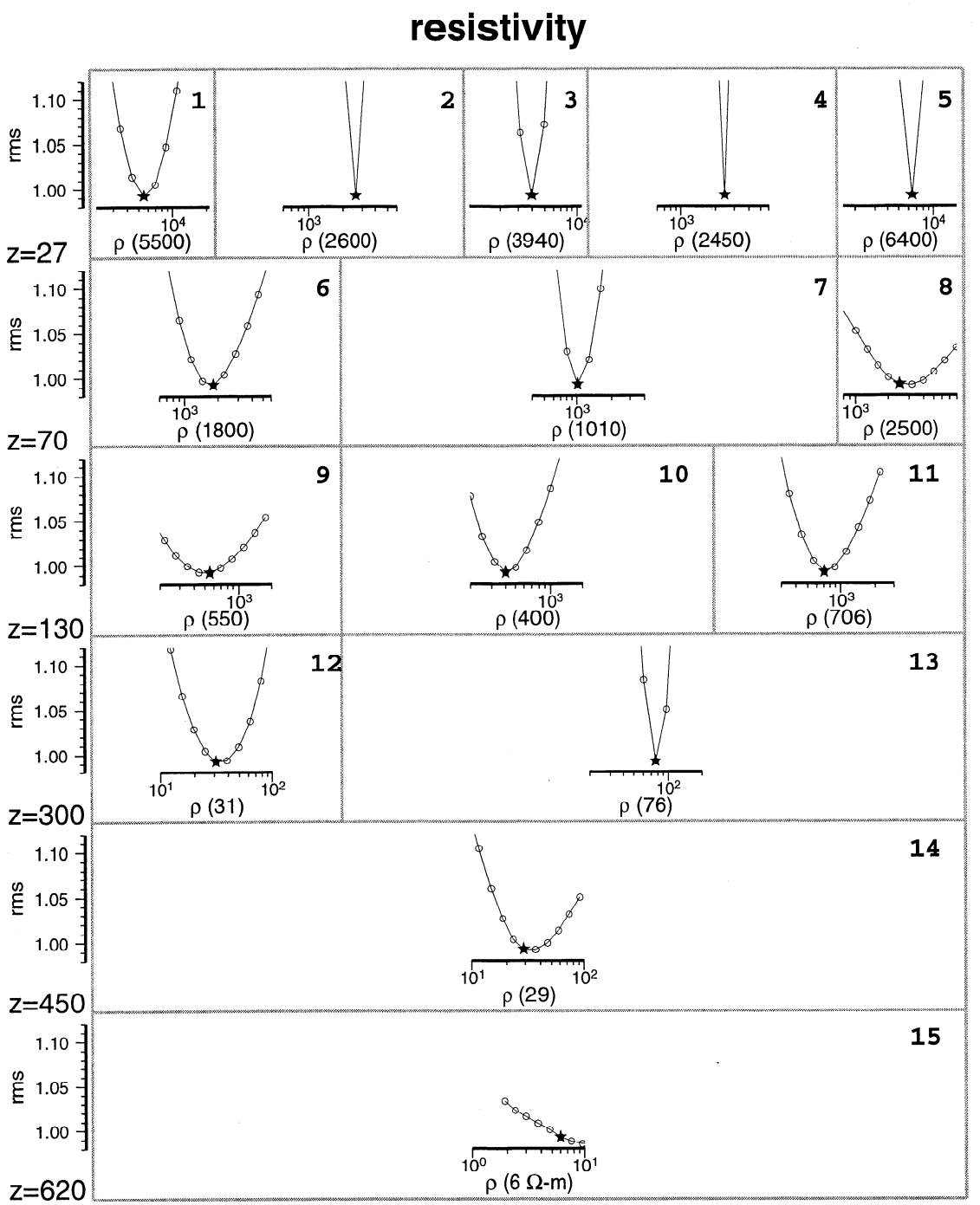

Figure 6a. Sensitivity analysis of the resolution of optimum model parameters by computing the change in the mistfit (rms) when all parameters are kept fixed except the resistivity of any block in the heterogeneous part of the model (in the central zone of Plate 1 top). The stars stand for the values used in the model (Plate 1) and the corresponding parameter value is in parentheses.

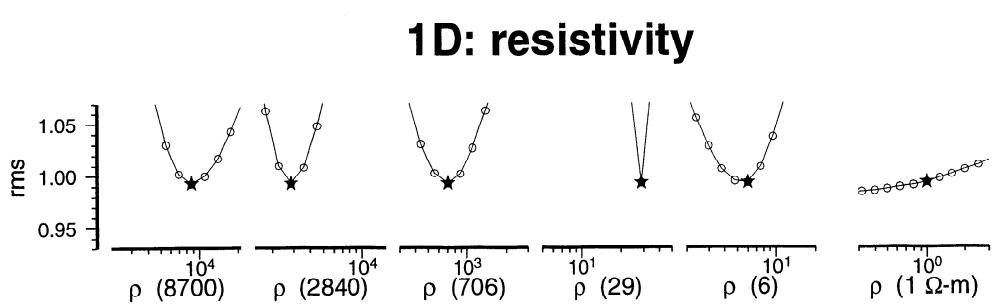

Figure 6b. The resistivity of any layer of the 1-D model.

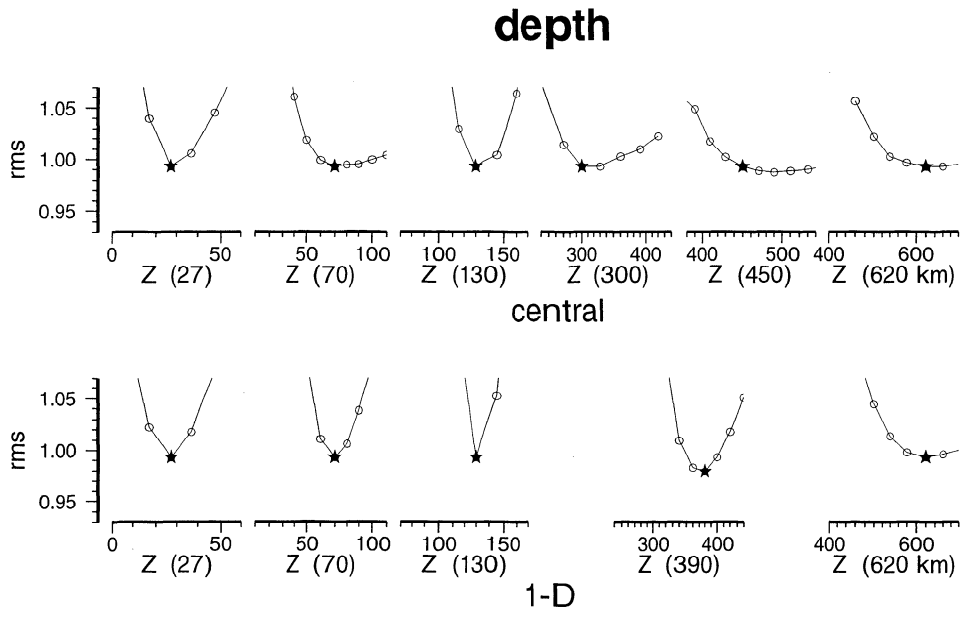

Figure 6c. The depths (top) of the blocks in the central area and (bottom) of the layers in the 1-D model.

This is illustrated in Figure 6c by the variation of the misfit with the thickness of each layer in the model presented in Plate 1. Some thicknesses are not well resolved, particularly at the greater depths. However, given the optimum resistivities in Figure 6a, most of the shallower block sizes are reasonably well constrained.

This analysis suggests that the main features depicted in the model of Plate 1 are required by the data. The new 1-D model beneath S6 has a 130 km resistive lid. At 400 km, the resistivity decreases sharply and decreases again below 620 km. In the central zone, heterogeneities are observed beneath the active area southeast of the island of Tahiti. The medium is slightly more conductive down to about 130 km with respect to the mean mantle as measured at site S6 at the same depth. Note that the width of the most conductive part decreases with depth. Between 130 km and 300 km, the resistivity increases from S10 to S13. On this side, the resistivity is higher than the one in the corresponding 1-D mantle at station S6. This resistor is required by the data at the 95% level (Figure 6). Between 300 and 400 km, the data do not allow significant lateral variation of the resistivity in the central part of the model. In fact, the resistivity structure is close to that of the starting mantle model. However, between 400 and 450 km the resistivity in the central part of the model is required to be higher than in the outlying mantle (Figure 6). This suggests a deepening of the vertical conductivity contrast in the central zone with respect to the more distant mantle.

4.3.2 Three-dimensional over 2-D modeling. The use of a 2-D model to explain the data implies that the structure shown in Plate 1 extends off of the locus of active volcanism. The question addressed now is the sensitivity of the data, in particular at station S16, to an interruption of the model ahead of the swell. If the structure follows from a classical hotspot mechanism, the mantle southeast of S16 should be normal with more or less the same structure as beneath S6. However, the data suggest that the mantle signature observed beneath the Teahitia swell extends ahead of S16. How far ahead? To answer this question, we used the 3-D algorithm of *Mackie et al.* [1993] to convert the 2-D model that we have obtained into a 3-D structure. The central part of the 3-D model is made of the 2-D medium from Plate 1. The limits of the central part are shown in Figure 7a. The model is bounded to the SW, NE and SE by the 1-D model from station 6. The boundary condition to the NW is 2-D and is therefore the continuation of the 2-D model from Plate 1. The details about the 3-D algorithm and the setup of the model are given by *Mackie et al.* [1993].

The 3-D response for this model was calculated with the SE bound (Figure 7a) at different distances from station 16. For each calculation, the resulting response was compared to the TE and TM data (Figure 5). Figure 7b (left) presents the variation of the misfit between the model and the data at S16 versus the distance of the SE bound to that station. Figure 7b (right) depicts the misfit for all stations with respect to this distance. In both cases, the misfit increases rapidly above the 95% confidence level for distances less than 100-150 km. This suggests that the heterogeneous mantle structure must extent ahead of S16 for at least 100-150 km.

5. Discussion

The electrical structure beneath the Society Islands hotspot obtained from the analysis of MT data suggests that an active plume is upwelling in an otherwise fairly homogeneous mantle. The heterogeneities are elongated along a N130±10°E direction (Figure 4), in approximate agreement with the actual spreading direc-

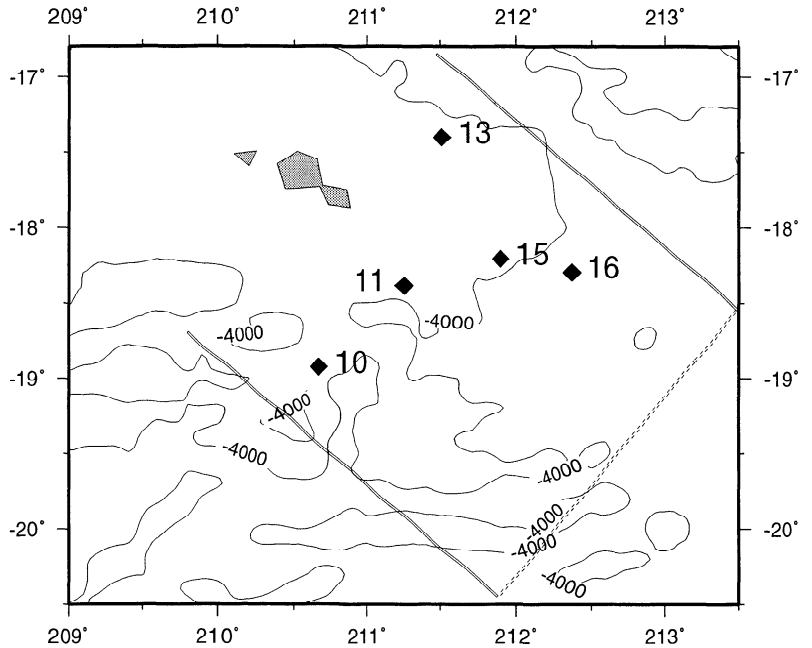

Figure 7a. Localization of the limits of the central part of the 2-D model (shown in Plate 1). Minimum distance from the stations of the southeast bound of the model (obtained by 3-D modeling).

tion (N115±5°E) of the Pacific plate and the direction of Society Islands chain (Figures 1a and 1b) [*Diraison et al.*, 1991]

The NE-SW width of the heterogeneous area is about 270 km. The NE bound is constrained by the data from stations 6 and 13. The SW bound is only constrained by the data from station 10. To the SE, a direct limit is not available, but the minimum distance of the extension of a possible plume to the SE was constrained from the data at station 16 by 3-D modeling to be 100-150 km (Figures 7a and 7b). If a circular cross section for a plume centered beneath Moua Pihaa is assumed, the approximate diameter is given by the NE-SW limits. This would also be in accordance with the data at station 16 since the plume's SE boundary would be far enough away to have a small influence. Note that the plume radius of about 135 km inferred beneath the Society Islands is close to the value suggested by *Wolfe et al.* [1997] beneath Iceland.

The electrical structure of the outlying and presumably normal mantle determined from the data at station 6 (Figure 8) has features comparable to the electrical oceanic mantle found in places in the North Pacific Ocean of different age [*Filloux*, 1980; *Oldenburg*, 1981; *Tarits*, 1986; *Tarits and Jouanne*, 1990]. The upper resistive layers (down to 110-130 km) may be attributed to a cold lithosphere overlying a more conductive asthenosphere. In the North Pacific, a cool-

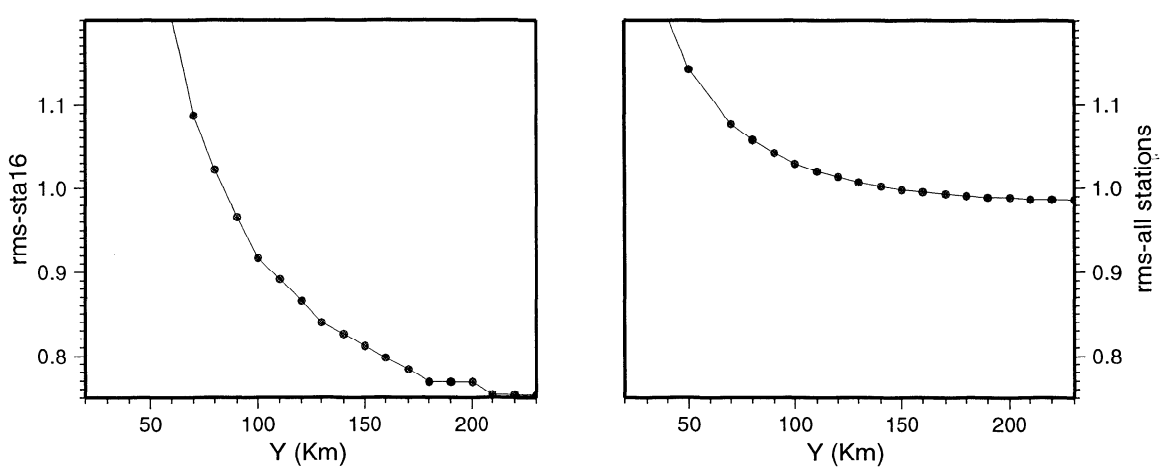

Figure 7b. Variation of the misfit (rms) between the model and data (left) at station 16 and (right) at all stations versus the distance of the 3-D southeast bound to station 16.

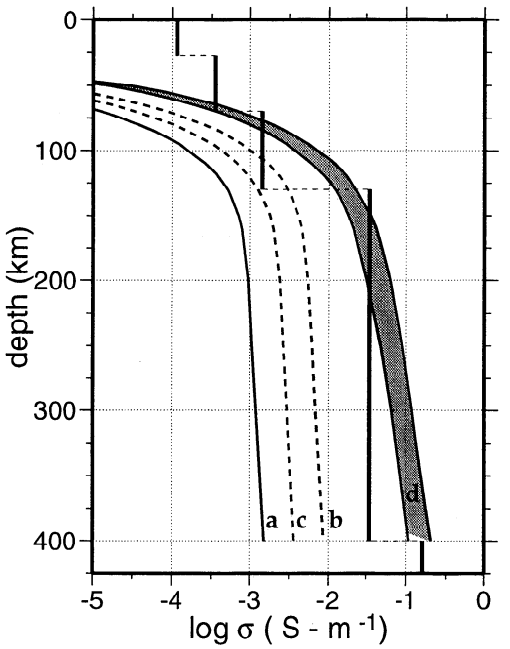

Figure 8. Resistivity profile beneath station 6 compared to laboratory resistivity models. Curve a, for dry olivine (taken from relation (10)); curves b and c, for olivine with 1% melt fraction with distribution in tubes (totally connected melt fraction) and distribution defined by Archie's law (partially interconnected melt fraction) respectively; and curve d, for Hashin-Shtrikman bounds for olivine saturated in hydrogen (or water). See text for details.

ing half-space model fits the observations well assuming that the base of the electrical lithosphere corresponds to the wet solidus of peridotite [e.g., *Tarits*, 1986; *Tarits and Jouanne*, 1990]. The magnetic anomaly record indicates that the lithosphere around Tahiti is 70±5 Ma [*Talandier and Okal*, 1987]. A similar age is found for the seafloor at station 6. Taking the half-space cooling model and prescribing the thermal diffusivity to be 1.13×10^{-6} m^2 s^{-1} [*McKenzie*, 1967], and the temperature of the upwelling mantle beneath the spreading center to be 1300°C [e.g., *Levill and Sandwell*, 1996], and considering that the bottom of the lithosphere is defined by the 1100-1200°C isotherms [*Wyllie*, 1988a], the thickness of the thermal lithosphere under station 6 would range from 100 km to 125 km.

The electrical lithosphere beneath station 6 is thicker than the electrical lithosphere identified in areas of similar age in the North Pacific [e.g., *Tarits*, 1986; *Tarits and Jouanne*, 1990]. If the drop in resistivity noticed at 110-130 km in depth was associated with melting and/or the presence of volatiles [e.g., *Oldenburg*, 1981; *Tarits*, 1986], the solidus should correspond to drier conditions at the same temperature (1100-1200°C) than the ones suggested for the North Pacific.

A large number of measurements of the electrical conductivity of dry olivine as a function of temperature have been done [e.g., *Shankland and Duba*, 1990; *Tyburczy and Roberts*, 1990]. These measurements were reviewed by *Constable et al.* [1992], who summarize these for the temperature range 750-1500°C by the relation

$$\sigma = 10^{2.402}e^{-1.6eV/kT} + 10^{9.17}e^{-4.25eV/kT} \quad (10)$$

where k is Boltzmann's constant and T is the absolute temperature.

A geotherm may be constructed for the lithosphere using parameters previously described and connected continuously to an adiabatic gradient of 0.3°C/km [*Turcotte and Schubert*, 1982] down to 400 km depth.

Using this estimation of the temperature in the upper mantle in (10), we obtained an upper mantle 1 to 2 orders of magnitude more resistive than the 1-D model (under station S6; see Figure 8, curve a). This has previously been observed in other deep magnetotelluric soundings carried out, for instance, in the North Pacific [*Tarits and Jouanne*, 1990; *Lizarralde et al.*, 1995].

The dry solidus temperature is higher than the estimated value, so it is not possible to have melting. However, if small fractions of volatiles (CO_2 and H_2O) are present, the position of the mantle solidus ("wet") can vary significantly. For a wet solidus with 0.1% of H_2O [*Ringwood*, 1975], the geotherm intersects it between 80 and 150 km depth, and for a wet solidus with 0.4% of H_2O and 5% CO_2 [*Wyllie*, 1988a], the geotherm intersects between 80 and 280 km. Using the partial melt fraction as a function of pressure and temperature given by *Ringwood* [1975] for the case of 0.1% of water and extrapolating this function for Wyllie's wet solidus, we find the maximum melt fraction is 1%.

The conductivity of bulk (solid and melt) is strongly dependent not only on melt fraction but also on the way that the melt is connected. We have considered two models for the melt geometry, one is the tube model of *Grant and West* [1965], which is based upon a system containing fluid-filled tubes along grain edges (for the case of totally connected melt fraction):

$$\sigma = \frac{1}{3}f\sigma_m + (1-f)\sigma_s \quad (11)$$

where σ_m and σ_s are the melt and solid phase conductivies, respectively, and f is the fraction of melt. Another case is only partially interconnected based on a modified form of Archie's law given by *Hermance* [1979]. In this model the conductivity is

$$\sigma = \sigma_s + (\sigma_m - \sigma_s)f^a \quad (12)$$

Following the argument of *Heinson and Constable* [1992], we consider a value of the melt fraction exponent $a = 1.5$, appropiate for upper mantle. We used the *Tyburczy and Waff* [1983] equation for the conductivity of the melt, obtained by measurement of electrical conductivity of Hawaiian tholeitic melt down to an equivalent depth of 80 km. The resulting resistivities are represented in Figure 8 curves b and c for equations (11) and (12), respectively.

At shallow and intermediate depths (<80-100 km) these models are highly resistive. The present data do not exclude these values because long-period seafloor

MT cannot resolve the upper bound of the resistivity in this depth range (Figure 2b). In the depth range 100-130 km, the theoretical resistivity model (with 1% and the tube model of *Grant and West* [1965]) fits the observed resistivity profile very well, providing that fluids are present. The structure beneath the lithosphere agrees with a mean compositional mantle. There is no evidence in the data for intense reheating in this area of the South Pacific.

At the lower part of the asthenosphere and between this and transition zone, the presence of 1% of melt is not enough to justify the high conductivities. At a depth of 250 km, we would need a melt fraction between 6.3% and 7.6% using the geometry of melt described by equations (11) and (12), respectively, but this amount of melt is unlikely to remains gravitationally stable in the mantle [*McKenzie*, 1984]. It is probable that the melt conductivity is being underestimated, as the presence of water in the melt may significantly increase its conductivity by providing a more mobile charge carrier, as proposed by *Lizarralde et al.* [1995].

The presence of water in the mantle may also act to increase mantle conductivity by supplying mobile charge carriers in the form of H^+ ions [*Karato*, 1990]. We perform a comparable analysis to that of *Lizarralde et al.* [1995] for the maximum influence of dissolved water-derived hydrogen on mantle conductivity. We have considered the conductivity of olivine at the H^+ solubility limit and assumed that this volumetrically dominant phase is interconnected and controls mantle conductivity. In Figure 8 we present Hashin-Shtrikman bounds (curves d) for saturated isotropic olivine (for calculation details, see *Lizarralde et al.* [1995]). The electrical structure, presumably normal mantle, at station 6 may be explained by an isotropic upper mantle nearly saturated (at a depth of 250 km 38% to 74% of a fully saturated mantle) in hydrogen (or water) or with the presence of melt.

At greater depths in the mean mantle model (Plate 1), the resistivity decreases significantly at about 400 km. This is in agreement with the depth of the olivine-spinel transition in the upper mantle [*Wajeman*, 1988, and references therein]. There also seems to be a resistivity decrease at about 600-650 km, but this is not well resolved by the data. Laboratory experiments show that the conductivity indeed increases sharply in the transition zone because of the olivine/spinel phase transition. A decrease of resistivity both at 400 km and 660 km has been observed with several deep magnetotelluric soundings carried out both in land and at sea. For instance, at Cartty Lake, Ontario, Canada, *Schultz et al.* [1993] observed a strong increase in conductivity between 400 and 456 km, and at Tucson, Arizona, *Egbert and Booker* [1992] observed an increase to 0.2-0.3 S m^{-1} between 300 and 600 km. *Egbert and Booker* [1992] showed that the data allow, but do not require, this increase to occur as a step at the olivine-spinel phase transition at 400 km depth.

The central part of the model presented in Plate 1 is clearly different from the mean mantle model found beneath station 6. The drop in resistivity at about 400 km in the mean mantle model is depressed to about 450 km. Given the positive Clapeyron slope of the phase transition [*Wyllie*, 1988a], this would correspond to an increase of temperature of about 350°C. This may be evidence for the upwelling of hot material from deep within the Earth. At depths greater than 450 km, no further differences are observed because the data are no longer sensitive to changes in the resistivity structure.

The upper 130 km of the central part of the model (between stations 13 and 10, Plate 1) shows weak heterogeneities. These heterogeneities seem to be correlated with the active hotspot area at the surface and to the plume at depth. It is not possible from these data to conclude that the lithosphere is thinned. There is a slight decrease in resistivity between 30 and 70 km in depth beneath stations 11 and 13. If we consider that the melting region is mainly located at the base of the lithosphere [*Wyllie*, 1988a], it is possible to determine the melt temperature in the lithosphere by assuming an adiabatic gradient of the melt in the lithosphere (we take 1°C/km based on the values of *McKenzie and Bickle* [1988]) and by considering the known eruption temperature of hotspot lavas. Maxi-

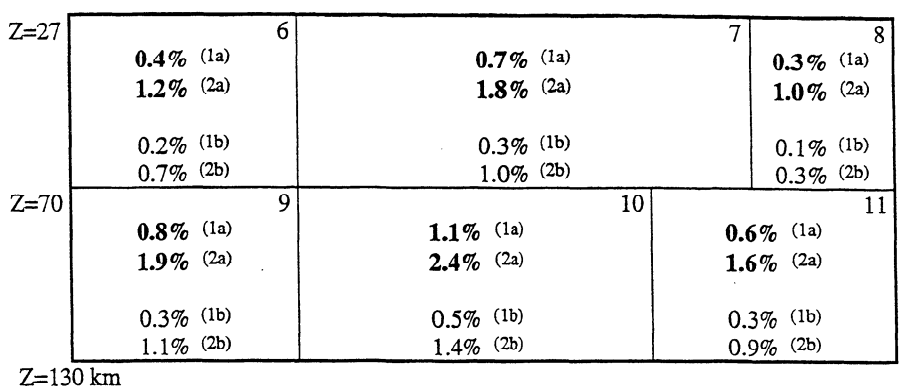

Figure 9. Computed melt fractions with: (1) taken from equation (11); (2) taken from equation 12; (a) taken for lavas temperature 1100°C and (b) for lavas temperature 1200°C. The numbers at top right of any cell are the block numbers at Plate 1.

mum temperature values of 1190°C and 1270°C have been reported for the "picritic" flows of Hawaii and Iceland, respectively [*Ceuleneer et al.*, 1993]. For the Society hotspot lavas, we take two possibles values, 1200°C and 1100°C. We have considered two possible melt distributions: partially interconnected (equation (12)) and melt-filled tubes along grain edges (equation (11)). The fraction of melt needed to obtain the observed conductivites in the central zone are presented in Figure 9. Knowing that the Iceland and Hawaii hotspots have more volcanic activity than the Tahiti hotspot, it is possible that the lava temperatures are lower in Tahiti (i.e., closer to 1100°C rather than 1200°C). So, the preferred bounds in fraction of melt would be those reported in bold in Figure 9.

Between 130 and 300 km in the center of Plate 1, the asthenosphere is laterally heterogeneous. We observe a higher resistivity beneath the most active zone (Figure 2 and Plate 1) than in the mean mantle to the northeast. This is apparently contradictory with the presence of rising hot material which ought to correlate with a decrease in resistivity. A melt and volatile depleted fraction of the mantle could be a possible explanation. When the melt and the volatiles are extracted, the residual material may become more resistive than the surrounding mantle because the material resistivity would then be closer to the resistivity of dry olivine. *Phipps Morgan* [1997] proposed a model of melting yielding volatile-depleted mantle beneath mid-ocean ridges to explain why there is no obvious relationship between the rate of hotspot volcanism on seafloor and crustal age. However, this mechanism would hold at much shallower depths than beneath Teahitia. The question of whether or not a fraction of rather deep mantle may be depleted so that the resistivity increases in spite of the increase in temperature is related to the larger problem of melting at great depth in the presence of volatiles.

Based on the magnetotelluric data, there is no evidence for an intense thermal mechanism acting over the whole superswell area as defined by *McNutt* [1998]. *Hofmann and White* [1982] and *Thompson* [1992] have proposed that such regions in the mantle could be anomalously rich in volatiles. *Bonatti* [1990] suggested that the origin of the Azores could be due to an anomalous volatile fraction in the mantle. *McNutt* [1998] suggested that as an alternative to a thermal explanation, the slow seismic shear wave velocity observed in the superswell region from the surface down to 450 km [*Su*, 1992] could be caused by the presence of volatiles. These volatiles may be transported into the mantle by hydrous minerals, particularly the dense hydrous magnesium silicates (DHMS) and some nominally anhydrous minerals from subducted oceanic lithosphere [*Bell and Rossman*, 1992; *Thompson*, 1992]. Water released by dehydration of DHMS can be stored in K-amphibole and β-Mg^2SiO^4 [*Thompson*, 1992]. This water from dehydration reactions could be stored in other hydrous minerals that are stable in the regions of the mantle through which they pass, depending on the relative amounts of water and trace cations such as potassium [*Thompson*, 1992]. The presence of water coming from subduction zones is supported by the geochemical signature in ocean island basalts (OIB) of the recycling of continental and oceanic sediments and crust-derived material via subduction zones [*Hofmann and White*, 1982; *Cohen and O'Nions*, 1982; *Zindler et al.*, 1982; *Zindler and Hart*, 1986]. The present volatile concentration in the mantle may also have been retained from the earliest phases of the Earth's accretion [*Ahrens*, 1989]. *Wyllie* [1988a] observed that there are high-pressure stable DHMS in the mantle away from subduction zones. The volatiles may be in higher local concentrations than in the rest of the mantle [*Hofmann and White* 1982; *Bell and Rossman*, 1992]. According to these authors, this could contribute to the source region of ocean island basalt.

Numerous experiments have shown that water considerably lowers the melting temperatures of rocks under pressure [e.g., *Olafsson and Eggleer*, 1983; *Ringwood*, 1975; *Davies and Stevenson*, 1992]. However, the experimental data extend no deeper than about 200 km. Some authors [e.g., *Wyllie*, 1988a; *Thompson*, 1992] have extrapolated these results to about 600-800 km in depth. Different types of soliduses can exist: saturated, undersaturated with all the water stored in a hydrous mineral, or anhydrous. The first and the last cases are extremes. They correspond to lower and upper bounds on the melting temperature, respectively [*Wyllie*, 1988b]. The solidi also depend on the formation of hydrous minerals, like amphibole generated in peridotite by reaction water [*Wyllie*, 1988b].

If the system is water-saturated, the solidus is about 500°C lower than the dry solidus for the upper mantle and through the transition zone [*Thompson*, 1992]. However, as noted by *Hirth and Kohlstedt* [1996], the solubility of water in olivine increases by a factor of about 3 with an increase in pressure from 0.3 to 1.0 GPa. Thus the percentage of saturated olivine decreases with an increase in pressure (hence depth), but the coefficient for partitioning of water into the melt actually increases with pressure. Due to preferential partitioning of water into the melt, even small amounts of melt can significantly decrease the concentration of water in the solid assemblage [*Hess*, 1992]. A mantle region with an anomalously high volatile concentration associated with a thermal anomaly may lead to melting at great depth [*Wyllie*, 1988b]. As the first melt is extracted, it depletes the region of volatiles, which will probably stop the melting at these depths by increasing the solidus temperature.

6. Conclusions

In this paper, seafloor magnetotelluric instruments data were used to image the mantle beneath the active Teahitia hotspot, French Polynesia. In order to adequately describe this active area while also being able to characterize deep structure on a larger scale, the magnetotelluric instruments were placed in a tight cluster around the active area with an additional remote site placed to the northeast toward the Tuamotu chain.

The magnetotelluric response functions after removing the distortion due to bathymetric and island effects

are consistent with a two-dimensional structure, around the active area, surrounded by an otherwise fairly homogeneous mantle one-dimensional structure.

In the electrical structure of normal mantle (one-dimensional mantle), (1) we observe an upper resistive layer (down to 110-130 km) which may be attributed to the lithosphere. The lithosphere overlies a more conductive asthenosphere. At greater depths, the resistivity decreases significantly at about 400 km. This is in agreement with the depth of the olivine-spinel transition in the upper mantle. There also seems to be a resistivity decrease at about 600-650 km, but this is not well resolved by the data. (2) In the depth range 100-130 km, the theoretical resistivity model, with 1% melt and a tubes model for its distribution, explains the observed resistivity profile very well. In the lower part of the asthenosphere and between this and the transition zone, the presence of 1% of melt is not enough to justify the high conductivities. These may be explained by an isotropic upper mantle nearly saturated in hydrogen (or water) or with the presence of melt if its conductivity is increased by the presence of water in it. (3) There is no clear evidence in the data for intense reheating and thinning of the lithosphere in this area of the South Pacific, but the presence of fluids seems to be needed to explain the resistivity profile.

The central structure of the model is clearly different from the mean mantle model. In this structure (1) we observe a heterogeneous mantle region elongated along a N130±10°E direction, in agreement with the actual spreading direction (N115±5°E) of the Pacific plate. We associate this structure, which is about 270km in diameter, with the hotspot plume. (2) There is no evidence for lithospheric thinning, but it is globally more conductive than a normal lithosphere, with various heterogeneities. We associate these heterogeneities with the presence of melt (between 1 and 2.4%) which is maximum at the bottom of the lithosphere, between 70 and 130 km deep and in the central region which corresponds to the most active volcanic zone on the surface (Figure 2 and Plate 1). (3) Between 130 and 300 km, the asthenosphere is laterally heterogeneous, with a more resistive structure than in the mean mantle (one-dimensional structure at site 6). This higher resistivity is beneath the most active zone (Figure 2 and Plate 1). This is apparently contradictory with the presence of rising hot material which ought to correlate with a decrease in resistivity, but a melted and volatile depleted fraction of the mantle could be a possible explanation. (4) The drop in resistivity observed in the mean mantle model at about 400 km is depressed to about 450 km. This would correspond to an increase of temperature of about 350°C. This may be the evidence for the upwelling of hot material from deep within the earth. At depths greater than 450 km, no further differences are observed because the data are no longer sensitive to changes in the resistivity structure.

Acknowledgments. The authors thank Lizarrald, J. Ingrin, H. Toh and an anonymous reviewer for their useful comments and sugestions. This work was supported at SIO by NSF grant OCE88-17710. This is WHOI contribution 9713. Rita Nolasco was supported by JNICT-Portugal grant "Projecto Ciência-BD/2201".

References

Ahrens, T. J., Water storage in the mantle, *Nature, 342,* 122-123, 1989.

Bell, D. R., and G. R. Rossman, Water in Earth's mantle: The role of nominally anhydrous minerals, *Science, 255,* 1391-1397, 1992.

Berdichevsky, M. N., and V. I. Dmitriev, Distortion of magnetic and electric field by near surface lateral heterogeneities, *Acta Geod. Geophys. Montan. Acad. Sci. Hung., 11,* 447-483, 1976.

Bonatti, E., Not so hot "hot spot" in the oceanic mantle, *Science, 250,* 107-111, 1990.

Burke, K., and J. T. Wilson, Hotspot on the Earth's surface, *Sci. Am., 235,* 46-57, 1976.

Calmant, S., The elastic thickness of the lithosphere in the Pacific Ocean, *Earth Planet. Sci. Lett., 85,* 277-288, 1987.

Calmant, S., and A. Cazenave, The effective elastic thickness unde the Cook-Austral and Society Islands, *Earth Planet. Sci. Lett., 77,* 187-202, 1986.

Calmant, S., and A. Cazenave, Anomalous elastic thickness of the oceanic lithosphere in the south- central Pacific, *Nature, 328,* 236-238, 1987.

Cazenave, A., B. Lago, K. Dominh, and K. Lambeck, On the rreponse of the ocean lithosphere to sea-mount loads from Geos3 satellite radar altimeter observations, *Geophys. J. R. Astron. Soc., 63,* 233-252, 1980.

Ceulcneer, G., M. Monnereau, M. Rabinowicz, and C. Rosemberg, Thermal and petrological consequences of melt migration within mantle plumes, *Philos. Trans. R. Soc. Lond. on, Ser. A, 342,* 53- 64, 1993.

Chave, A. D., and J. T. Smith, On electric and magnetic galvanic distortion tensor decompositions, *J. Geophys. Res., 99,* 4669-4682, 1994.

Chave, A. D., and D. J. Thomson, Some comments on magnetotelluric response function estimation, *J. Geophys. Res., 94,* 14,215-14,202, 1989.

Cheminée, J. L., R. Hekinian, J. Talandier, F. Albarède, C. W. Devey, J. Francheteau, and Y. Lancelot, Geology of an active hot spot: Teahitia-Mehetia region in central Pacific, *Mar. Geophys. Res., 11,* 27-50, 1989.

Cohen, R. S., and R. K. O'Nions, Identifiction of recyced continental material in the mantle from Sr, Nd and Pd isotope investigations, *Earth Planet. Sci. Lett., 61,* 73-84, 1982.

Constable, S., T. J. Shankland, and A. Duba, The electrical conductivity of an isotropic olivine mantle, *J. Geophys. Res., 97,* 3397-3404, 1992.

Cornaglia, B., Synthèse des données géophysiques Nazca-Pacifique, thèse de doctorat, Univ. de Paris VII, 1995.

Counil, J. L., Le Nouël, and M. Menvielle, Associate and conjugate directions concepts in magnetotellurics, *Ann. Geophys., (B2) 4,* 115-130, 1986.

Crough, S. T., Thermal origin of mid-plate hot-spot swells, *Geophys. J. R. Astron. Soc., 55,* 451-469, 1978.

Davies, J. H., and D. H. Stevenson, Physical model of source region of subduction zone volcanics, *J. Geophys. Res., 97,* 2037-2070, 1992.

Detrick, R. S., and S. T. Crough, Island subsidence, hot spot, and lithosphre thinning, *J. Geophys. Res., 83,* 1236-1244, 1978.

Diraison, C., H. Bellon, C. Leotot, R. Brousse, and H. G. Barczus, L'alignement de la Société (Polynésie française): volcanologie, géochronologie, proposition d'un modèle de point chaud, *Bull. Soc. Géol. Fr., 162(3),* 479-496, 1991.

Doucet, D., and Pham Van Ngoc, Généralisation et optimalisation de la méthode des différences finies pour la modélisation en magnétotellurique (MT), *Geophys. Prospect., 32,* 292-316, 1984.

Duncan, R. A., and D. A. Clague, Pacific plate motions recorded by linear volcanic chain, in *The Ocean Basins and Margins*, edited by A. E. M. Nairn, F. G. Stelhi, and S. Uyeda, pp. 98-121, Plenum Press, New York, 1985.

Duncan, R. A., and I. McDougall, Linear volcanism in French Polynesia, *J. Volcanol. Geotherm. Res., 1,* 197-229, 1976.

Egbert, G. D., and J. R. Booker, Very long period magnetotellurics at Tucson observatory: Implications for mantle conductivity, *J. Geophys. Res., 97,* 15,099-15,112, 1992.

Filloux, J. H., Ocean-floor magnetotelluric soundig over north central Pacific, *Nature, 269,* 297-301, 1977.

Filloux, J. H., Magnetotellurics and related electromagnetic investigations in geophysics, *Rev. Geophys., 17,* 282-297, 1979.

Filloux, J. H., Magnetotelluric soundings over the northwest Pacific may reveal spacial dependence of depth and conductance of the asthenosphere, *Earth Planet. Sci. Lett., 46,* 244-252, 1980.

Filloux, J. H., Instrumentation and experimental methods for oceanic studies, in *Geomagnetism*, vol. 1, edited by J. Jacobs, pp. 143-246, Academic, San Diego, Calif., 1987.

Filmer, P. E., M. K. McNutt, and C. J. Wolfe, Elastic thickness of the lithosphere in the Marquesas and Society Islands, *J. Geophys. Res., 98,* 19,565-19,577, 1993.

Fischer, G., and B. V. LeQuang, Topography and minimization of the standard deviation in one- dimensional magnetotelluric, *Geophys. J. R. Astron. Soc., 67,* 257-278, 1981.

Grant, F. S., and G. F. West, Interpretation Theory in Applied Geophysics, McGraw-Hill, New York, 1965.

Groom, R. W., and R. C. Bailey, Decomposition of magnetotelluric impedance tensors in the presence of local three-dimensional galvanic distortion, *J. Geophys. Res., 94,* 1913-1925, 1989.

Heinson, G., and S. Constable, The electrical conductivity of the oceanic upper mantle, *Geophys. J. Int., 110,* 159-179, 1992.

Hékinian, R., P. Stoffers, J. L. Cheminée, R. Mühe, D. Bideau, and N. Binard, Submarine intraplate volcanism in the South Pacific: Geological setting and petrology of the Society and the Austral regions, *J. Geophys. Res., 96,* 2109-2138, 1991.

Hermance, J. F., The electrical conductivity of materials containing partial melts: A single model from Archie's law, *Geophys. Res. Lett., 6,* 613-616, 1979.

Hess, P. C., Phase equilibria constraints on the origin, in *Mantle Flow and Melt Generation at Mid-Ocean Ridges, Geophys. Monogr., Ser.*, Vol. 71, edited by J. P. Morgan, D. K. Blackman, and J. M. Sinton, pp. 67-103, AGU, Washington, D.C., 1992.

Hirth, G., and D. L. Kohlstedt, Water in the oceanic upper mantle: implications for rheology, melt extraction and the evolution of the lithosphere, *Earth Planet. Sci. Lett., 144,* 93-108, 1996.

Hofmann, A. W., and W. M. White, Mantle plumes from ancient oceanic crust, *Earth Planet. Sci. Lett., 57,* 421-436, 1982.

Jarrard, R., and D. A. Clague, Implications of Pacific island and seamounts ages for the origin of volcanic chains, *Rev. Geophys., 15,* 57-76, 1977.

Karato, S., The role of hydrogen in the electrical conductivity of the upper mantle, *Nature, 347,* 272-273, 1990.

Knittle, E., R. Jeanloz, and G. L. Smith, Thermal expansion of silicate perovskite and stratification of the Earth's mantle, *Nature, 319,* 214-215, 1986.

Levill, D. A., and D. T. Sandwell, Modal depth anomalies from multibeam bathymetry: Is there a South Pacific superswell?, *Earth Planet. Sci. Lett., 139,* 1-16, 1996.

Lizarralde, D., A. Chave, G. Hirth, and A. Schultz, Northeastern Pacific mantle conductivity profile from long-period magnetotelluric sounding using Hawaii-to-California submarine cable data, *J. Geophys. Res., 100,* 17, 837-17, 854, 1995.

Mackie, R. L., T. R. Madden, and P. E. Wannamaker, Three-dimensional magnetotelluric modeling using difference equations: Theory and comparisons to integral equation solutions, *Geophysics, 58,* 215-226, 1993.

Mammerickx, J., E. Herron, and L. Dorman, Evidence for two fossil spreading ridges in the southeast Pacific, *Geol. Soc. Am. Bull., 91,* 263-271, 1980.

McDougall, I., and R. A. Duncan, Linear Volcanic chains; recording plate motions?, *Tectonophysics, 63,* 275-295, 1980.

McKenzie, D., Some remarks on heat flow and gravity anomalies, *J. Geophys. Res., 72,* 6261-6273, 1967.

McKenzie, D., The generation and compaction of partial molten rock, *J. Petrol., 25,* 713-765, 1984.

McKenzie, D., and M. J. Bickle, The volume and composition of melt generation by extension of the lithosphere, *J. Petrol., 29,* 625-679, 1988.

McNutt, M. K., Superswells, *Rev. Geophys., 36,* 211-244, 1998.

McNutt, M. K., and K. M. Fisher, The South Pacific Superswell, in *Seamounts, Islands, and Atolls, Geophys. Monogr. Ser.*, Vol. 43, edited by B. H. Keating, pp. 25-34, AGU, Washington, D.C. 1987.

McNutt, M. K., and A. V. Judge, The Superswell and mantle dynamics beneath the South Pacific, *Science, 248,* 969-975, 1990.

McNutt, M. K., and H. W. Menard, Lithospheric flexure and uplifted atolls, *J. Geophys. Res., 83,* 1206-1212, 1978.

Menvielle, M., J. C. Rossignol, and P. Tarits, The coast effect in terms of deviated electric currents: A numerical study, *Phys. Earth Planet. Inter., 28,* 118-128, 1982.

Moberly, R., and J. F. Campbell, Hawaiian hotspot volcanism mainly during geomagnetic normal intervals, *Geology, 12,* 459-463, 1984.

Morgan, W. J., Convenction plumes in the lower mantle, *Nature, 230,* 42-43, 1971.

Okal, E. A., J. Talandier, K. A. Sverdrup, and T. H. Jordan, Seismicity and tectonic stress in the south central Pacific, *J. Geophys. Res., 85,* 6479-6495, 1980.

Olafsson, M., and D. H. Eggler, Phase relations of amphibole-carbonate, and phlogopite-carbonate peridotite: Petrologic constraints on asthenosphere, *Earth Planet. Sci. Lett., 64,* 305-315, 1983.

Oldenburg, D. W., Conductivity structure of oceanic upper mantle beneath the Pacific plate, *Geophys. J. R. Astron. Soc., 65,* 359-394, 1981.

Parker, R. L., The inverse problem of electromagnetic induction: Existence and construction of solutions based on incomplete data, *J. Geophys. Res., 86,* 4421-4428, 1980.

Parker, R. L., and K. A. Whaler, Numerical methods for establishing solutions to the inverse problem of electromagnetic induction, *J. Geophys. Res., 85,* 9574-9584, 1981.

Parsons, B., and S. Daly, The relationship between surface topography, gravity anomalies, and temperature structure of convection, *J. Geophys. Res., 88,* 1129-1144, 1983.

Pautot, G., Analyse structural de l'archipel des Tuamotus: Origine volcanique-tectonique (hot-spot or not?), paper presented at 3rd RAST, Soc. Géol. Fr., Montpellier, France, April 23-25, 1975.

Phipps Morgan, J., The generation of a compositional lithosphere by mid-ocean ridge melting and its effect on sub-

sequent off-axis hotspot upwelling and melting, *Earth Planet. Sci. Lett., 146,* 213- 232, 1997.

Phipps Morgan, J., W. J. Morgan, and E. Price, Hotspot melting generates both hotspot volcanism and a hotspot swell?, *J. Geophys. Res., 100,* 8045-8062, 1995.

Ribe, N. M., and U. R. Chistens, Three-dimensional modeling of plume-lithosphere interation, *J. Geophys. Res., 99,* 669-682, 1994.

Ringwood, A. E., *Composition and Petrology of the Earth's Mantle*, McGraw-Hill, New York, 1975.

Robinson, E. M., The topographic and gravitational expression of density anomalies due to melt extration in the uppermost oceanic mantle, *Earth Planet. Sci. Lett., 90,* 221-228, 1988.

Schultz, A. , R. D. Kurtz, A. D. Chave, and A. G. Jones, Conductivity discontinuities in the upper mantle beneath a stable craton, *Geophys. Res. Lett., 20,* 2941-2944, 1993.

Shankland, T. J., and A. G. Duba, Standard electrical conductivity of isotropic, homogeneous olivine in the temperature range 1200°-1500°C, *Geophys. J. Int., 103,* 25-31, 1990.

Sleep, N. H., An analytical model for a mantle plume fed by boundary layer, *Geophys. J. R. Astron. Soc., 90,* 119-128, 1987.

Stein, C. A., and D. H. Abbott, Heat flow constraints on the South Pacific superswell, *J. Geophys. Res., 96,* 16,083-16,100, 1991.

Su, W. J., The three-dimensional shear-wave velocity structure of the Earth's mantle, Ph.D. thesis, Havard Univ., Cambridge, Mass., 1992.

Talandier, J., and G. T. Kuster, Seismicity and submarine volcanic activity in French Polynesia, *J. Geophys. Res., 81,* 936-948, 1976.

Talandier, J., and E. A. Okal, The volcanoseismic swarms of 1981-1983 in the Tahiti-Mehetia area, French Polynesia, *J. Geophys. Res., 89,* 11,216-11,234, 1984.

Talandier, J., and E. A. Okal, Crustal structure in Society and Tuamotu Islands, French Polynesia, *Geophys. J. R. Astron. Soc., 88,* 499-528, 1987.

Tarits, P., Conductivity and fluids in the oceanic upper mantle, *Phys. Earth Planet. Inter., 42,* 215-226, 1986.

Tarits, P., and V. Jouanne, Résultats de sondages magnétotelluriques sous-marins et structure thermique de la lithosphère océanique, *Bull. Soc. Géol. Fr. 6(6),* 921-931, 1990.

Tarits, P., and M. Menvielle, Etude du champ magnétique anormal d'origine intralithosphérique, *Can. J. Earth Sci., 20,* 537-547, 1983.

Tarits, P., V. Jouanne, M. Menvielle, and M. Roussignol, Bayesian statistics of non-linear inverse problems: Example of the magnetotelluric 1-D inverse problem, *Geophys. J. Int., 119,* 353- 368, 1994.

Terra, A., Modélisation électromagnétique de deux plaques minces hétérogènes et son application à l'étude de la croûte et du manteau, thèse de doctorat, Univ. de Paris VII, 1993.

Thompson, A. B., Water in the Earth's upper mantle, *Nature, 358,* 295-302, 1992.

Thomson, D. J., and A. D. Chave, Jackknife error estimates for spectra, coherences, and transfer functions, *Advances in Spectral Analysis and Array Processing*, edited by S. Haykin, pp. 58-113, Prentice-Hall, Englewood Cliffs, N. J., 1991.

Turcotte, D. L., and G. Schubert, *Geodynamics*, John Wiley, New York, 1982.

Tyburczy, J. A., and J. J. Roberts, Low-frequency electrical response of polcrystalline olivine compacts: grain boundry transport, *Geophys. Res. Lett., 17,* 1985-1988, 1990.

Tyburczy, J. A., and H. S. Waff, Electrical conductivity of molten basalt and andesite to 25 kilobars pressure: Geophysical significance and implications for charge transport and melt structure, *J. Geophys. Res., 88,* 2413-2430, 1983.

Vasseur, G., and P. Weidelt, Bimodal electromagnetic induction in non-uniform thin sheets with an application to northern Pyrenean induction anomaly, *Geophys. J. R. Astron. Soc., 51,* 669-690, 1977.

Vozoff, K., The magnetotelluric method in the exploration of sedimentary basins, *Geophysics, 37,* 98-141, 1972.

Wajeman, N., Detection of underside P reflections at mantle discontinuites by stacking broadband data, *Geophys. Res. Lett., 15,* 669-672, 1988.

Watts, A. B., An analysis of isostasy in the world's oceans, Hawaiian-Emperor seamount chain, *J. Geophys. Res., 83,* 5985-6004, 1978.

Watts, A. B., J. H. Bodine, and N. M. Ribe, Observations of flexure and the geological evolution of the Pacific Ocean basin, *Nature, 283,* 532-537, 1980.

Weidelt, P., Electromagnetic induction in three dimensional structures, *J. Geophys., 41,* 85- 109, 1975.

White, S. N., A. D., Chave, and J. H. Filloux, A look at galvanic distortion in the Tasman Sea and Juan de Fuca Plate, *J. Geomagn. Geoelectr., 49,* 1373-1386, 1997.

Wilson, J. T., A posible origin for the Hawaiian Islands, *Can. J. Phys., 41,* 863-870, 1963.

Wolfe, C. J., I. T. Bjarnason, J. C. VanDecar, and S. C. Solomon, Seismic structure of the Iceland mantle plume, *Nature, 385,* 245-247, 1997.

Wyllie, P. J., Magma genesis, plate tectonics, and chemical differentiation of the Earth, *Rev. Geophys., 26,* 370-404, 1988a.

Wyllie, P. J., Solidus curves, mantle plumes, and magma generation beneath Hawaii, *J. Geophys. Res., 93,* 4171-4181, 1988b.

Zindler, A., and S. Hart, Chemical geodynamics, *Annu. Rev. Earth Planet. Sci., 14,* 493-571, 1986.

Zindler, A., E. Jagoutz, and S. Goldstein, Nd, Sr and Pd isotopic systematics in three component mantle: a new perspective, *Nature, 298,* 519-523, 1982.

A. C. Chave, Department of Geology and Geophysics, Woods Hole Oceanographic Institution, Woods Hole, MA 02543. (e-mail: achave@whoi.edu.).

J. H. Filloux, Scripps Institution of Oceanography, University of California, San Diego, La Jolla, CA 92037. (e-mail: jfilloux@ucsd.edu).

R. Nolasco and P. Tarits, CNRS UMR "Domaines Océaniques," Institut Universitaire Européen de la Mer, Université de Bretagne Occidentale, 1 place Nicolas Copernic, Technopole Brest-Iroise, 29280 Plouzané, France. (e-mail: maria@univ-brest.fr; tarits@univ-brest.fr).

(Received November 21, 1997; revised May 8, 1998; accepted June 17, 1998.)